Article

The Optimization of Waterproof and Drainage Design and an Evaluation of the Structural Safety of Tunnels in Weak Watery Strata

Zelin Zhou [1,2,3]**, Xingyu Zhu** [1,2]**, Chuantian Zheng** [1,2]**, Zhiqiang Zhang** [1,2,]*** and Heng Zhang** [1,2]

[1] State Key Laboratory of Intelligent Geotechnics and Tunnelling, Southwest Jiaotong University, Chengdu 610031, China; zhouzelin2023@163.com (Z.Z.)
[2] School of Civil Engineering, Southwest Jiaotong University, Chengdu 610031, China
[3] China 19th Metallurgical Corporation, Panzhihua 617000, China
* Correspondence: clarkchang68@163.com; Tel.: +86-13980066612

Abstract: The surrounding rock and high water pressure in weak watery strata have adverse effects on the mechanical properties of tunnel support structures. In order to optimize the anti-drainage design of tunnels in weak watery strata and evaluate their structural safety, this paper relies on the Taidacun Tunnel of the China–Laos Railway to carry out field monitoring research. A dual-field fluid–solid coupling calculation model is established to optimize the tunnel's waterproof and drainage design, combined with a bending moment curvature model to evaluate structural safety. The main conclusions are as follows: Under the action of high water and soil pressure, the structural safety margin of the water-rich fine sand section of the Taidacun Tunnel is small, and waterproof and drainage design optimization is required. Combined with the proposed average pressure reduction coefficient, the influence of the water level and annular blind pipe spacing on the water pressure of the lining is proved, and then the optimal annular blind pipe spacing in the water-rich area of the tunnel is determined. A structural safety evaluation method based on the bending moment curvature model is proposed. Two models of elastic beam and moment–curvature beam are used to analyze the mechanical characteristics and optimization effects of the structure under optimal annular blind pipe spacing.

Keywords: weak watery stratum; field monitoring; fluid–solid coupling; average pressure reduction coefficient; bending moment–curvature model

1. Introduction

Deeply buried tunnels in water-rich areas have unlimited recharge from groundwater sources due to large burial depth and high water pressure. Problems such as lining cracking and water seepage due to high pressure often occur during tunnel operation. In order to ensure the safe and efficient operation of tunnels, it is necessary for tunnel support structures in water-rich areas to have certain waterproof, drainage, and safety performance [1,2]. Water plugging and drainage restriction are common treatment measures in the construction of tunnels in water-rich strata. Under the guidance of this design concept, the tunnel waterproof and drainage system consists of a water-plugging grouting ring, initial support, secondary lining, and a drainage system [3,4]. Scholars have carried out a lot of research on the existing waterproof and drainage system and the structural safety under the action of high water pressure and surrounding groundwater seepage.

In terms of waterproof tunnel and drainage design research, Bao et al. [5] proposed a composite waterproof and drainage system and studied the changes in the seepage field of traditional waterproofing and drainage systems and composite waterproof and drainage systems under different blockage conditions through model experiments to verify the

effectiveness of the system. Duan et al. [6] studied the distribution law of seepage pressure within different distances from the tunnel wall based on analytical derivation, verified the accuracy of the theoretical solution, and optimized the parameters of various parts of the composite lining. Fan et al. [7] studied the evolution of water pressure after lining, the vertical displacement of the reverse arch, and the failure characteristics of the structure under water pressure through setting up a seepage model test system. Zhang et al. [8] analyzed the characteristics of traditional waterproof drainage systems and proposed a new drainage structure through numerical simulation and indoor experiments. Zhao et al. [9] studied three optimization schemes for waterproofing and drainage through numerical simulation and model experiments. Zhang et al. [10] proposed a design method for waterproofing and drainage systems in tunnel lining to reduce interference with groundwater. Li et al. [11] proposed a new concept of a railway tunnel bottom drainage and precipitation system. The performance of the proposed drainage system is verified through a series of numerical analyses.

In the research on the safety of tunnel lining structures in water-rich areas, Wang et al. [12] developed a pressure-adaptive concrete lining for hydraulic tunnels with high water pressure and high ground water pressure based on the theory of thick-walled cylinders. He et al. [13] developed equipment to simulate external water pressure on the lining of a horseshoe tunnel and combined it with a finite-element numerical model to validate the proposed method through comparing relevant bending moments, thrust, and shear forces. Chen et al. [14] conducted experiments on tunnels under different static water head heights using a self-developed seepage model testing device and studied the distribution of seepage fields in small spacing tunnels in water-rich areas and its impact on structural mechanical behavior. Wu et al. [15] studied the long-term stress and structural deformation characteristics of water-rich loess tunnels through numerical simulation and field monitoring. Liu et al. [16] studied the damage behavior of tunnel lining based on numerical methods and proposed corresponding maintenance design methods for lining safety. Song et al. [17] developed a 1:10 large-scale test platform and determined the load on the lining model based on field-measured pressure data. The deformation evolution law, cracking mechanism, and failure process of the secondary lining of existing highway tunnels in loess strata has also been studied. Guo et al. [18] conducted a series of model tests to study the mechanical behavior of shield tunnel structures under the combined action of external soil water load and internal water pressure. Ding et al. [19] analyzed the safety of high-pressure tunnel lining with limited drainage based on the finite difference method. Huang et al. [20] studied the pressure and failure evolution of linings based on field monitoring and numerical methods.

To summarize, scholars have carried out abundant research on tunnel waterproof and drainage systems and the safety of secondary lining structures in water-rich areas. However, there are still deficiencies: (1) Existing studies mainly investigate the structural safety of different waterproof and drainage designs through model tests and numerical simulation methods. There are few experimental studies combined with the field monitoring of tunnels, and the reliability of the research results cannot be guaranteed. (2) The existing analysis and calculation methods for structural safety are often based on structural strain or stress test results, which require sensors to be buried in the structure in advance, and the cost of structural safety evaluation is high. Therefore, on the basis of existing research, on-site tunnel monitoring should be combined with numerical simulation, and the relationship between tunnel structural safety and waterproofing and drainage design parameters should be established to provide a basis for waterproofing and drainage design. In addition, a new safety factor evaluation method needs to be proposed to facilitate practical engineering applications and solve the problems of high cost and the need to bury sensors in advance in traditional methods.

In this paper, field monitoring of tunnels in water-rich areas is carried out to analyze the distribution characteristics of water and earth pressure on the tunnel structure and its evolution over time. The mechanical response law of the lining structure in the water-rich

fine sand section and the general surrounding rock section is compared and analyzed. A numerical model of fluid–solid coupling in water-rich tunnels is established. The average pressure reduction coefficient index is proposed to evaluate the pressure relief capacity of the waterproof and drainage system under different head heights and design parameters. Finally, the optimal drainage blind pipe spacing is determined. The mechanical characteristics of the lining structure were analyzed via comparing the two models of elastic beam and bending moment–curvature beam. A lining safety evaluation method based on the bending moment–curvature method was proposed to evaluate the safety of the lining structure under the optimized waterproof and drainage design. The conclusions of the study provide guidance for the waterproof and drainage design and structural safety evaluation analysis of tunnels in water-rich areas.

2. Tunnel Field Monitoring

2.1. Project Overview

The Yumo Line of China–Laos Railway is a Class I national electrified railway connecting Yuxi City and Mohan, Mengla County, in Yunnan Province, China, and an important part of the middle passage of the Pan Asian Railway. Its geographical location is shown in Figure 1. With a total length of 507 km and a design speed of 160 km/h, Yumo Line is one of the landmark projects of China's "the Belt and Road" construction. A total of 93 tunnels with a total length of 398 km are designed for the Yumo Line, of which the Taidacun Tunnel is a key control project, of the China–Laos Railway. It located in the southern section of the Hengduan Mountains, between Ning'er Station and Pu'er Station, with an inlet mileage of DK239 + 810 and an outlet mileage of DK245 + 625. The tunnel is a single-hole double-track tunnel with a total length of 5815 m and is designed as a single slope.
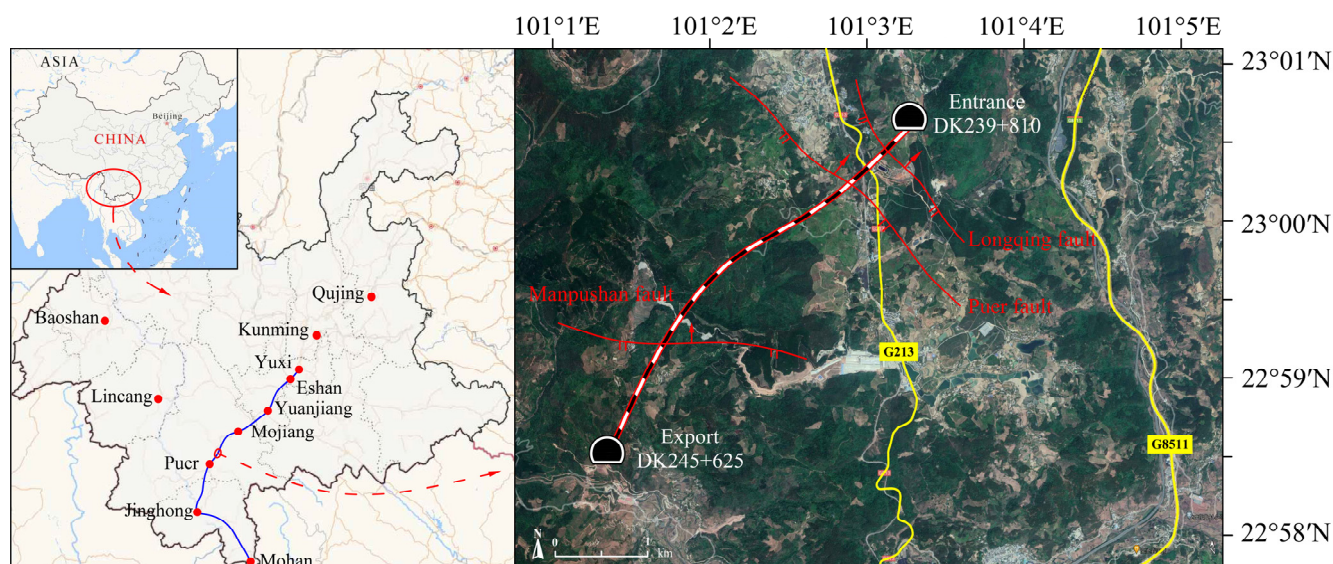

Figure 1. Overview of geographical location of Taidacun Tunnel on Yumo Line of China–Laos Railway.

2.2. Monitoring Program

The burial depth of the tunnel is relatively large, and the groundwater resources are abundant. During tunnel construction, water inrush is highly likely to occur. During the operation period of the tunnel, it is also highly prone to lining seepage and water leakage, which has a significant impact on the safety and applicability of the tunnel during the operation period. Groundwater mainly exists in weathered and structural fractures of the bedrock. The water abundance of groundwater is related to its lithology. Through

comprehensive geological exploration methods such as drilling and geophysical exploration, it is found that the lithology of the strata in the Taidacun Tunnel site area is mainly sandstone, mudstone, silty clay, and conglomerate. Among them, weathered fissures in mudstone are developed, but structural fissures are not developed. Due to the weak weathering resistance of the rock mass and obvious weathering, joint fissures are mostly filled with weathered mud, with small water storage space and weak water abundance. But, in sandstone and conglomerate, structural and weathered fractures are developed, resulting in good water abundance. The diagenesis of fine sand soil is poor, and when there is no groundwater, the surrounding rock has a certain degree of self stability. However, structural damage may occur under the infiltration of groundwater. In addition, under the influence of construction disturbance, the silty fine sand soil is easily transformed into loose sand, which sharply weakens the stability of the tunnel surrounding rock.

The distance between the circumferential blind pipes of the Taidacun Tunnel is 15 m, with a diameter of 100 mm. The diameter of the tunnel's longitudinal drainage blind pipe is 100 mm. The grouting ring is used for reinforcement in the water-rich section, so that the original groundwater seepage channels in the surrounding rocks within the grouting ring are blocked. The change in the flow direction of groundwater improves the stress state of the structure, which meets the drainage needs of normal surrounding rock sections in water-rich areas. However, further research is needed for fine sand formations with good water abundance. Therefore, in order to study the soil and water pressure and lining structural mechanical characteristics of the water-rich and fine sand formation section and the general section under the existing drainage design, three monitoring sections have been set up, with mileages of DK241 + 392, DK241 + 721, and DK242 + 976. The geological conditions of the Taidacun Tunnel and the specific mileages of the three monitoring sections are shown in Figure 2.
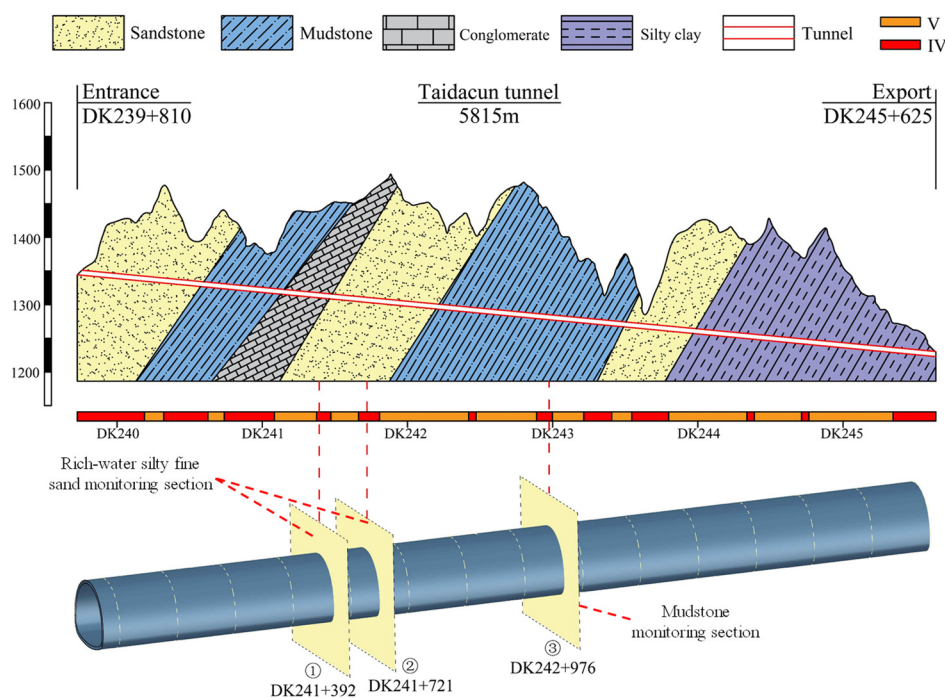
**Figure 2.** Geological profile and monitoring section settings.

The main contents of the field test include the following: (1) The pressure test of the surrounding rock between the surrounding rock and the primary support. Obtain the stress state and stress distribution characteristics of the support structure under different working conditions. (2) Pore water pressure test. Obtain the water pressure value and distribution law of the pore water pressure in each stage of the construction process. (3) Strain

test of the secondary lining molded concrete. Monitor the concrete strain, and then determine the value of the axial force and bending moment and its change law. Then, evaluate the safety of the lining structure.

The stress state of the initial support is complex. And the regularity of the internal force and safety factor of the initial support is weak. Moreover, after the secondary lining is constructed, the deformation and curvature of the initial support are difficult to obtain, and the cost of structural safety evaluation is high. In addition, under normal circumstances, the secondary lining of tunnels serves as a safety reserve for the tunnel. Its stress state directly affects the operational safety of the tunnel, so it is more reasonable to evaluate the secondary lining.

In order to grasp the overall distribution of water pressure, soil pressure, and structural internal force in each section, sensors are installed for monitoring at the arch crown, arch shoulder, arch waist, arch foot, and inverted arch of the lining. The specific sensor layout plan and field installation are shown in Figure 3. The numbers of each monitoring point are A~H from the vault to the arch foot.
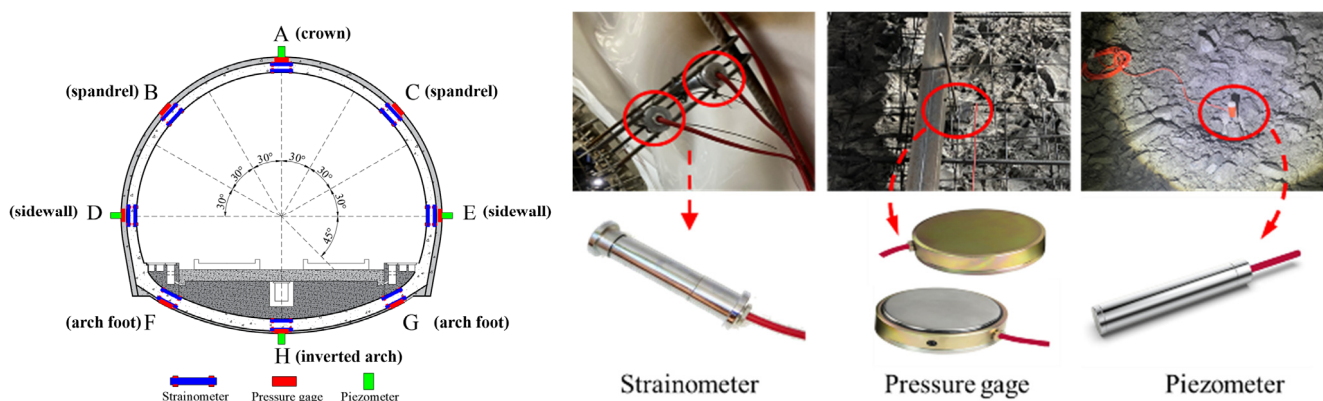
Figure 3. Sensor layout and installation.

2.3. Monitoring Results and Analysis

Continuously monitor the water pressure and soil pressure of the three sections until the monitoring data are basically stable. Then, draw the variation curve of water pressure and soil pressure, as well as a simplified diagram of the distribution of water pressure and soil pressure on the stabilized section, as shown in Figures 4–6.
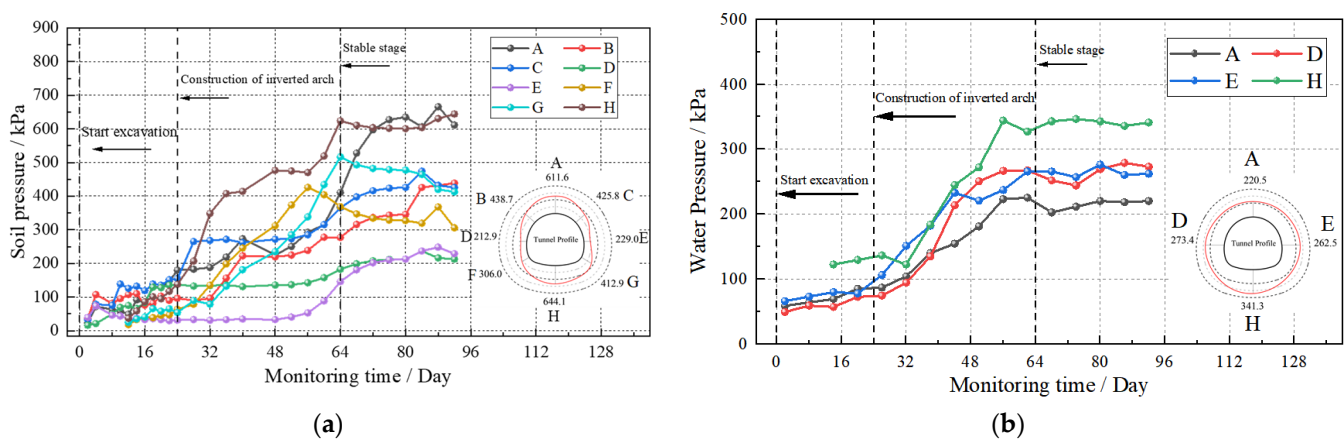
Figure 4. Section 1 monitoring data. (**a**) Earth pressure; (**b**) water pressure
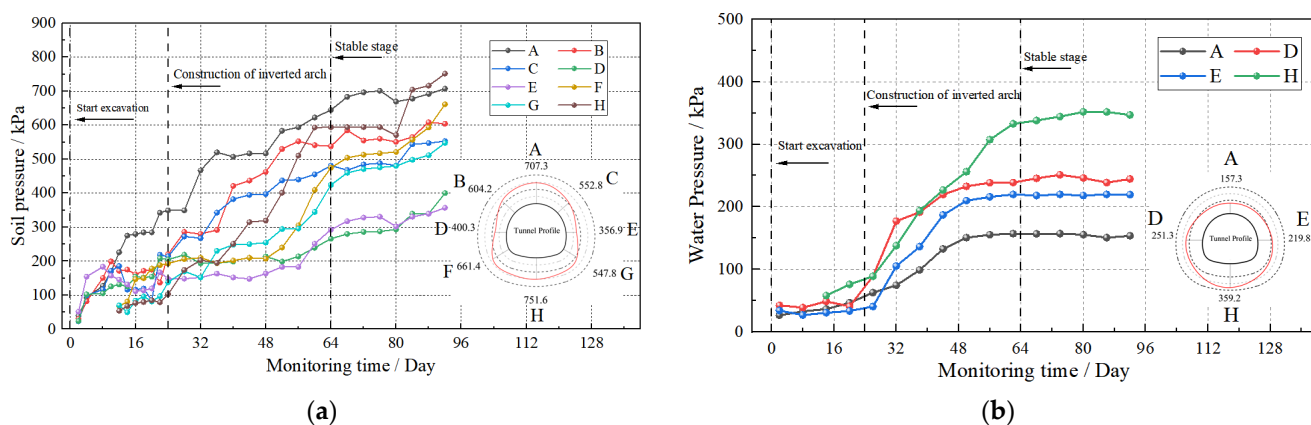
(a)

(b)

Figure 5. Section 2 monitoring data. (**a**) Earth pressure; (**b**) water pressure.
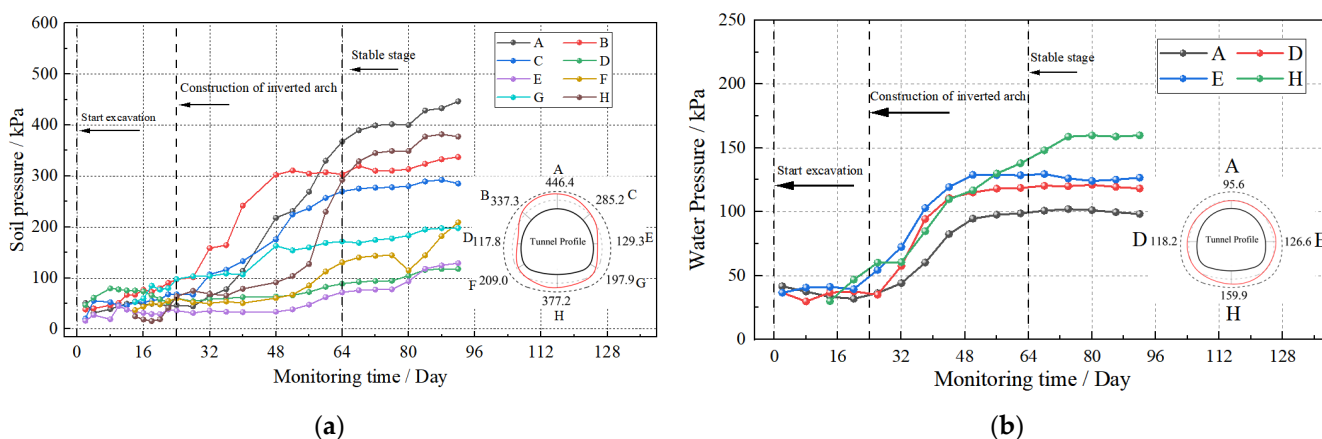

(a)

(b)

Figure 6. Section 3 monitoring data. (**a**) Earth pressure; (**b**) water pressure.

According to the changes in water and soil pressure of the tunnel during different periods measured on site, it can be seen that the changes in water and soil pressure on the support structures of the three sections go through three stages; they are the tunnel excavation stage, the secondary lining ring formation stage, and the later stable fluctuation stage (environmental impacts such as rainfall).

In the first stage, initial support is applied after tunnel excavation, and the supporting effect of the initial support gradually manifests with the increase in stiffness. The soil pressure of each section shows a slow upward trend, and at this time, the soil pressure of the arch crown and arch shoulder increases relatively faster. At this stage, the water pressure also slowly increases. In the second stage, after the construction of the secondary lining, due to the better load-bearing performance of the composite lining structure, the increase in surrounding rock pressure is accelerated. In addition, due to the closure of the lining structure, water pressure also increases rapidly.

During the later stable fluctuation period, the water and soil pressures at each section tend to stabilize. The overall distribution of soil pressure shows a distribution pattern of larger arch crown and inverted arch, with smaller side walls, and the maximum soil pressure of Sections 1 and 2 appears at the inverted arch, with values of 644.1 kPa and 751.6 kPa, respectively. The maximum soil pressure of Section 3 is at the arch crown, with a value of 446.4 Pa. The overall distribution pattern of water pressure is small from top to bottom, and the maximum water pressure of Sections 1–3 all occurs in the inverted arch, with values of 341.3, 339.2 kPa, and 159.9 kPa, respectively. The distribution patterns of water pressure and soil pressure in the three sections are roughly the same. From a numerical perspective, the water pressure and soil pressure of Monitoring Sections 1 and 2

in the water-rich fine sand formation are significantly higher than those of Monitoring Section 3 in the mudstone.

2.4. Safety Evaluation of Lining Structure

The secondary lining of the Taidacun Tunnel is made of C35 reinforced concrete, with a circumferential reinforcement of HRB400, a diameter of 25 mm, a spacing of 200 mm, and a lining thickness of 65 cm. The secondary lining concrete strain values of the three sections of the Taitacun Tunnel were monitored, and then the secondary lining bending moment M and axial force N were calculated using the formulae. The structural safety coefficients were then calculated to evaluate the safety of the tunnel. The lining structure is a compression bending component, and its mechanical behavior can be divided into small eccentric compression and large eccentric compression, as shown in Figure 7.
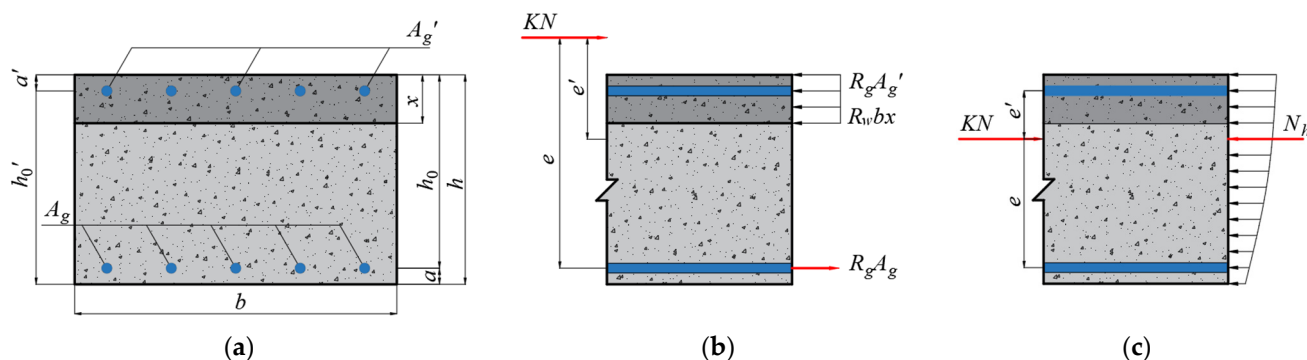
Figure 7. Stress mode of reinforced concrete under compression and bending. (**a**) Reinforced concrete cross-section; (**b**) stress diagram of large eccentric compression components; (**c**) stress diagram of small eccentric compression components.

The formula for calculating the safety factor of reinforced concrete structures is as follows [21].

When the rectangular section of reinforced concrete is subjected to small eccentric compression ($x > 0.55\,h$):

$$KNe \leq 0.5R_a bh_0^2 + R_g A_g' (h_0 - a') \tag{1}$$

When the rectangular section of reinforced concrete is subjected to large eccentric compression ($x \leq 0.55\,h$):

$$KN \leq R_w bx + R_g (A_g' - A_g) \tag{2}$$

In the above, A_g, A_g' is the cross-sectional area of longitudinal tensile and compressive steel bars; b is the calculative width, which is taken to be 1.0 m; x is the height of the reinforced concrete compression zone; R_a is the ultimate compressive strength of concrete; R_w is the ultimate flexural compressive strength of concrete; R_g is the calculated tensile or compressive strength of steel bars; h_0 is the effective height of the section (m).

Through the processing of the monitoring data of the internal force of the structure in the field, the structures are all in the state of small eccentric compression. This also shows that the groundwater pressure causes the structure to have a large axial force, which exhibits small eccentric compression. The distribution diagrams of the internal forces and safety factors of the secondary lining at three monitoring sections are shown in Figures 8–10.
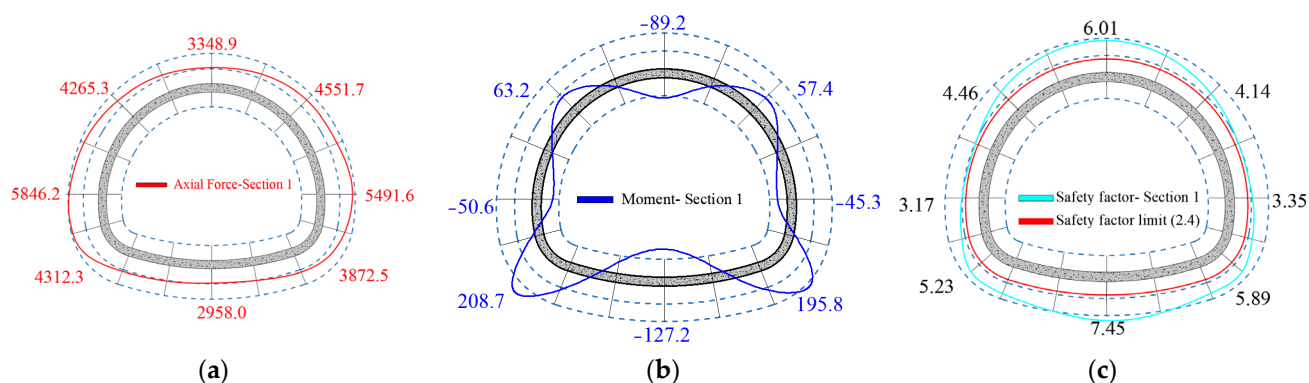
Figure 8. Internal force and safety factor of lining structure of Section 1. (**a**) Axial force (kN); (**b**) bending moment (kN·m); (**c**) safety factor.
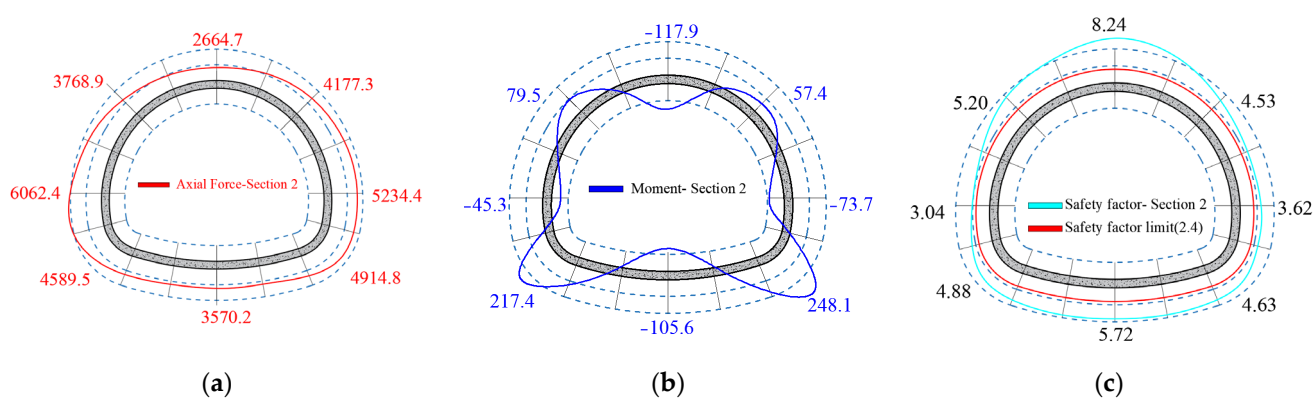
Figure 9. Internal force and safety factor of lining structure of Section 2. (**a**) Axial force (kN); (**b**) bending moment (kN·m); (**c**) safety factor
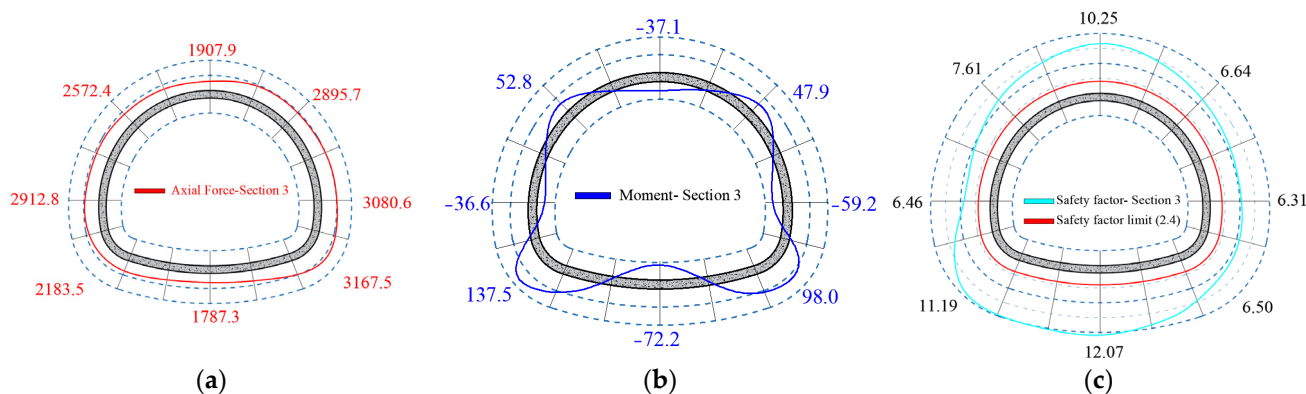
Figure 10. internal force and safety factor of lining structure of Section 3. (**a**) Axial force (kN); (**b**) bending moment (kN·m); (**c**) safety factor.

Based on the calculated internal force and safety factor of the lining, we can summarize some conclusions as follows.

The internal force of the lining structure is directly related to the load it bears. Due to the greater water and soil pressure on Sections 1 and 2 located in the water-rich and fine sand layer, their internal forces are also significantly greater than those on Section 3. Taking axial force as an example, the maximum axial forces of Sections 1 and 2 are 5846.2 kN and 6062.4 kN, respectively, located at the side wall position. But the maximum axial force of Section 3 is at the left wall foot, measuring 3366.2 kN. The bending moment distribution of the three sections is similar, with the maximum positive bending moments occurring at the arch foot position, measuring 208.7 kN·m, 248.1 kN·m, and 137.5 kN·m, and the

maximum negative bending moments are all located at the center of the inverted arch, measuring −127.2 kN·m, −105.6 kN·m, and −72.2 kN·m.

The safety factor of the lining calculated from Equations (1) and (2) shows that, in Section 3, the safety coefficient of the lining structure shows a situation where the arch crown and inverted arch are large and the side walls are small. In Sections 1 and 2, there is a pattern where the inverted arches are small and the side walls and arch crown are large. The safety factor calculated for Section 3 is significantly greater than the safety factor for the secondary lining of Sections 1 and 2, and according to field monitoring results, the safety factor of the tunnel lining is greater than the critical safety factor of 2.4 in the specifications. However, the safety margin for Sections 1 and 2 is insufficient, with the minimum values only being 3.17 and 3.04, so during tunnel operation, due to the degradation of structural mechanical properties such as cracking and water leakage, it is difficult to ensure structural safety.

According to the statistical results of cracks during the operation period of Taitacun Tunnel, although the structure is still in a safe condition, cracks have appeared in parts of the lining, as shown in Figure 11. No water leakage occurred after subsequent repairs. It can be seen that the safety margin of the lining structure is insufficient under the original waterproof and drainage design parameters.

(**a**)   (**b**)
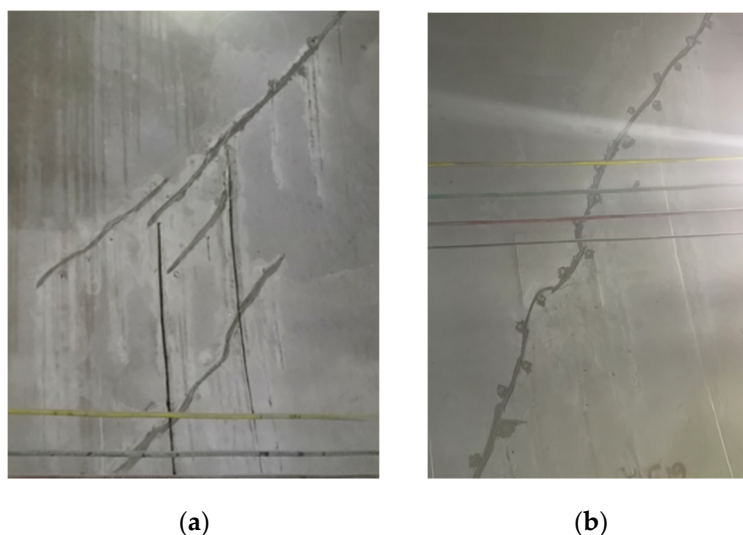
Figure 11. Secondary lining cracks. (**a**) Mileage DK241 + 397; (**b**) mileage DK241 + 750

Through the field monitoring and research of the tunnel structure mentioned above, it can be found that the internal force of the secondary lining structure of the tunnel in rich water and weak strata is greater than that of the general lining structure, significantly affecting the safety of the secondary lining structure. In addition, evaluating the safety of lining structures through the above methods is complex and not convenient for engineering applications, Therefore, it is necessary to optimize the design of waterproof and drainage of tunnels, and propose a more applicable safety evaluation method.

3. Distribution Pattern of Lining Water Pressure and Waterproof and Drainage Design during Operation Period

Most railway and highway tunnels require no seepage or leakage and must meet the first-level waterproof standard. However, the geological environment of long and deep tunnels built in mountainous areas is extremely complex, with groundwater levels consistently higher than those of tunnels, and if the drainage network system has a weak ability to relieve pressure on groundwater, its hydraulic effect will deteriorate the tunnel structure during operation, causing tunnel cracking and seepage of water during

operation. Therefore, analysis of the longitudinal blind pipe network of the tunnel ring and studying the influence of head height (external factors) and internal factors (circumferential blind pipe spacing) on the pressure relief capacity of drainage network systems to determine the optimal spacing of circular drainage blind pipes are necessary conditions for improving the waterproof and drainage performance of tunnels.

3.1. Establishment of a Numerical Model for Drainage Blind Pipe Seepage

To study the influence of drainage blind pipes on the stress distribution of lining structures during tunnel operation, a numerical model was established as shown in Figure 12. The Y-axis of the model is the longitudinal direction of the tunnel, the Z-axis is the burial depth direction, and the X-axis is the horizontal direction perpendicular to the tunnel. Considering boundary effects and model computational complexity, the distance from the tunnel to the upper, lower, and left and right boundaries of the model is set to be 50 m. Except for the top surface, radial constraints are applied to the other five surfaces, with a tunnel burial depth of 150 m. An overlying load is applied to the top surface of the model. The blue arrow in the figure represents boundary constraints, while the red arrow represents the load applied to the top surface of the model

(**a**)   (**b**)
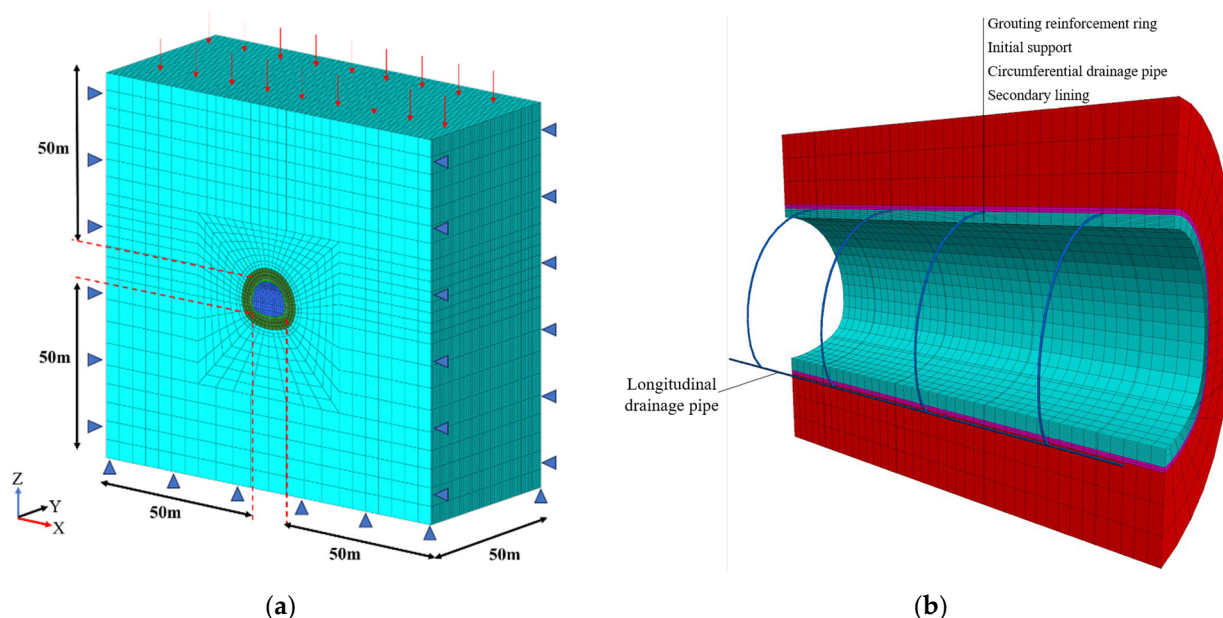
Figure 12. Model schematic diagram. (**a**) Schematic diagram of calculation model. (**b**) Schematic diagram of drainage network layout.

As shown in Figure 12, the surrounding rock of the numerical model adopts a constitutive model that meets the Mohr Coulomb yield criterion, and both the initial support and secondary lining structures adopt isotropic elastic constitutive models. Considering that the overall structure of the tunnel is subjected to water pressure, the groundwater level is selected as three types: 20 m, 40 m, and 60 m, and assuming that the groundwater level of the stratum where the tunnel is located remains unchanged in the calculation, the spacing between the circumferential drainage blind pipes is set to 8 m. Finally, the physical, mechanical, and hydraulic parameters of each part of the numerical model are shown in Table 1. Assign the parameters in the table to the numerical model and record the stress situation of the lining under different groundwater levels.

Table 1. Parameters of surrounding rock and support structure.

Category	Elastic Modulus,	Poisson's Ratio, μ	Cohesion, c (MPa)	Friction, φ (°)	Density, ρ (kg/m³)	Permeability Coefficient, K (cm/s)

	E (GPa)					
Mudstone	0.19	0.3	25	18	2000	—
Silty fine sand	0.07	0.35	0.0037	31	1837	8.76×10^{-3}
Initial support	3.4	0.2	—	—	2300	1×10^{-6}
Secondary lining	31.5	0.2	—	—	2500	—
Grouting area	0.8	0.31	0.12	35	2200	5×10^{-4}

3.2. Water Pressure Distribution of Lining with Drainage Blind Pipe

The drainage structure system can have a direct impact on the water pressure behind the tunnel lining. At the same time, the water pressure on the tunnel lining is also an important basis for evaluating the safety of the lining structure in water-rich strata. Therefore, the numerical model established for the layout of drainage blind pipes with a spacing of 8 m is taken as an example to study the stress characteristics and pore water pressure distribution characteristics of the secondary lining under water heads of 20 m, 40 m, and 60 m. The results obtained through numerical calculations are shown in Figures 13–15.
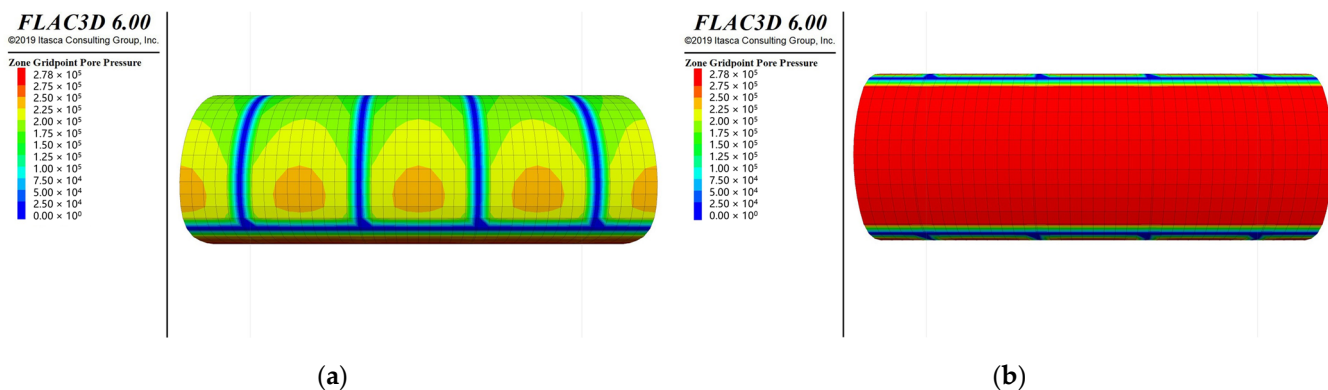

(**a**)

(**b**)

Figure 13. Cloud chart of water pressure behind the secondary lining with a groundwater level of 20 m above the arch (Unit: Pa). (**a**) Water pressure behind the secondary lining. (**b**) Water pressure behind the inverted arch.

(**a**)

(**b**)

Figure 14. Cloud chart of water pressure behind the secondary lining with a groundwater level of 40 m above the arch (Unit: Pa). (**a**) Water pressure behind the secondary lining. (**b**) Water pressure behind the inverted arch.
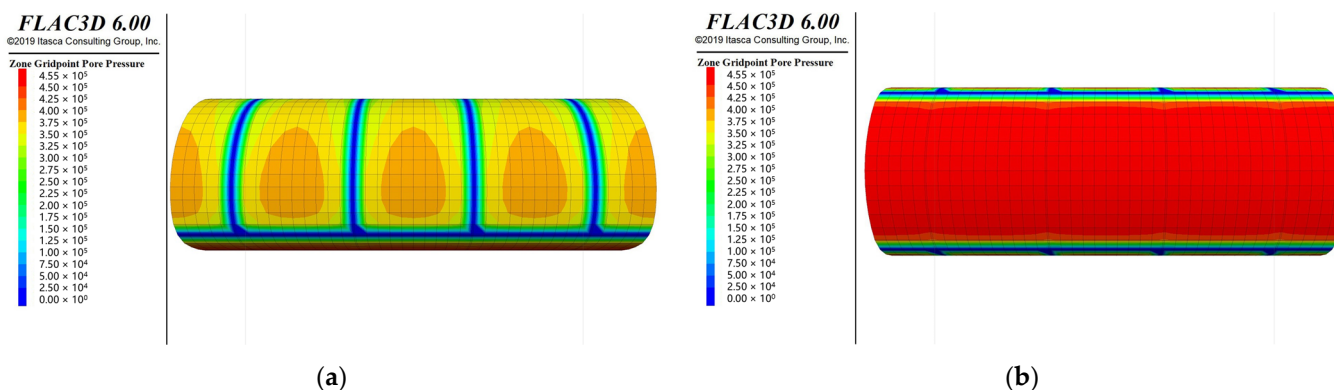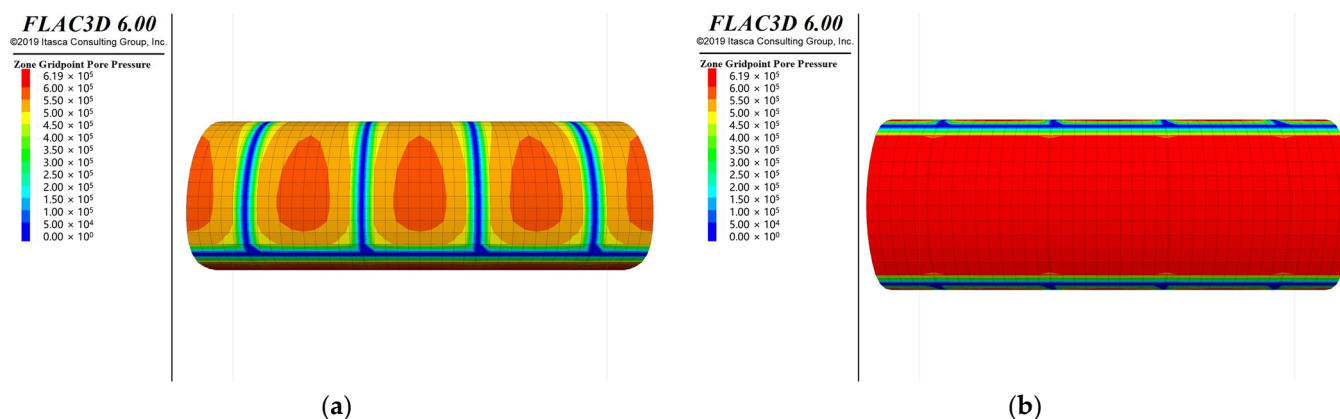
Figure 15. Cloud chart of water pressure behind the secondary lining with a groundwater level of 60 m above the arch (Unit: Pa). (**a**) Water pressure behind the secondary lining. (**b**) Water pressure behind the inverted arch.

Based on the analysis of the calculation results of the water pressure distribution behind the secondary lining in Figures 13–15, the following conclusions can be drawn.

The distribution of lining water pressure calculated through numerical simulation is similar to the distribution of water pressure obtained from field monitoring, which shows the characteristics of being small at the arch crown, large at the inverted arch, and gradually increasing water from the arch crown to the inverted arch. It proved the effectiveness and authenticity of the established numerical model.

The arrangement of circumferential and longitudinal blind pipes can significantly reduce the pore water pressure acting on the upper part of the lining. Due to the drainage effect of the drainage pipe, the pore water pressure acting on the area closer to the drainage blind pipe becomes smaller. From the figure, it can be seen that the minimum value of pore water pressure appears on both sides of the circumferential and longitudinal drainage blind pipes. Correspondingly, in the area far away from the drainage blind pipe, the pore water pressure in the area rapidly increases due to the weak drainage pressure relief effect of the drainage blind pipe.

The maximum value of pore water pressure occurs at the middle side wall near the arch foot of each circumferential blind pipe interval. Under the arrangement of drainage blind pipes with a spacing of 8 m, the maximum pore water pressure on the outer side of the upper secondary lining at water levels of 20 m, 40 m, and 60 m is 164.85 kPa, 334.75 kPa, and 506.05 kPa, respectively. The increase in pore water pressure from 20 m to 60 m is 207%, and the maximum values are all less than the calculated water pressure of the groundwater level line above the arch crown, which may indicate the arrangement of drainage blind pipes can reduce the impact of water pressure rise caused by groundwater level rise.

Comparing the pore water pressure of the lower inverted arch and the upper secondary lining, it can be seen that due to the lack of a layout of circular drainage blind pipes, the pore water pressure acting on the inverted arch is significantly greater than that of the upper secondary lining. Looking longitudinally along the tunnel, the arrangement of the secondary-lining circumferential and longitudinal blind pipes did not result in a significant decrease in pore water pressure at the same longitudinal position of the inverted arch compared to other parts; that is, there was basically no change in pore water pressure at the longitudinal direction of the inverted arch. It can be seen that under the spacing arrangement of 8 m drainage blind pipes, the maximum pore water pressures on the outer side of the inverted arch under the water level conditions of 20 m, 40 m, and 60 m are 278.53 kPa, 454.90 kPa, and 619.28 kPa, respectively, and the increase in pore water pressure from 20 m to 60 m is 122%, and the pore water pressure values at the inverted arch are greater than those of the upper secondary lining.

3.3. Research on the Reasonable Spacing of Drainage Blind Pipes in Tunnel during Operation Period

Based on the established numerical model, to study the reasonable spacing of drainage blind pipes in tunnels during operation, we set the longitudinal blind pipes in the tunnel drainage network system to be A100 drainage pipes. At the same time, in accordance with relevant industry requirements, design specifications related to waterproof and drainage design, and the actual difficulty of engineering construction, in numerical calculations, a total of 15 different operating conditions are set up under different conditions of circumferential blind pipe spacing and groundwater levels. The specific arrangement of the spacing between circumferential blind pipes is shown in Table 2.

Table 2. Numerical simulation conditions.

Working Condition	Distance between Circular Drainage Blind Pipes	Overburden Water Level on the Arch
1	3 m	
2	5 m	20 m
3	8 m	40 m
4	12 m	60 m
5	15 m	

3.3.1. Distribution of Lining Water Pressure under Different Spacing of Drainage Blind Pipes

Based on the set operating conditions, the pressure relief effect of drainage blind pipes with different spacing on the external water pressure of the lining structure is studied through analyzing the changes in water pressure behind the lining structure under different operating conditions. According to relevant research, over 20% of tunnels are mainly characterized by water leakage at the arch crown [22]. Therefore, this study mainly focuses on the arch as the research object. In numerical calculations, the pore water pressure on the outer side of the secondary lining at the arch crown was recorded under different circumferential blind pipe spacing, and we drew a curve of pore water pressure at the arch crown with different blind pipe spacing along the longitudinal direction of the tunnel, as shown in Figure 16.

(a)

(b)

(c)

(**d**)

(**e**)
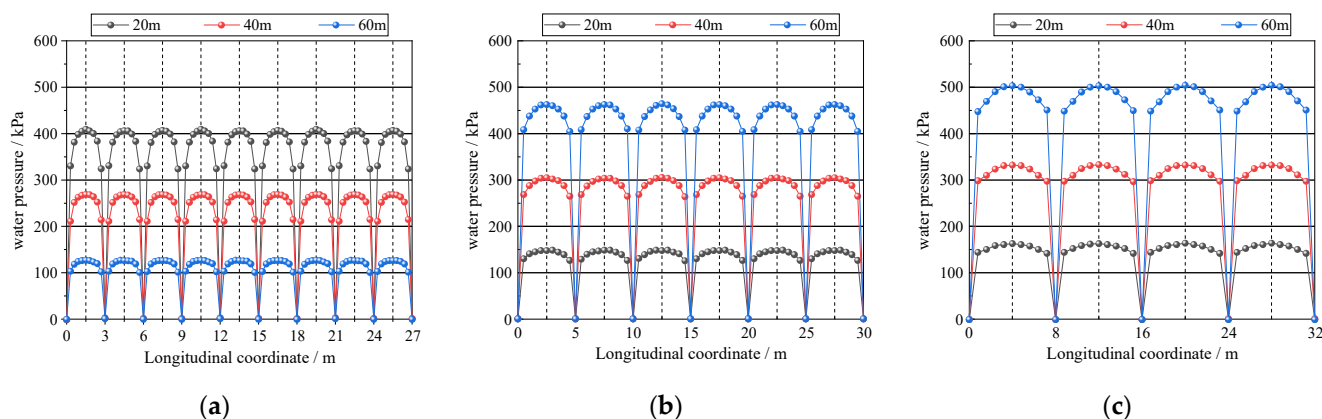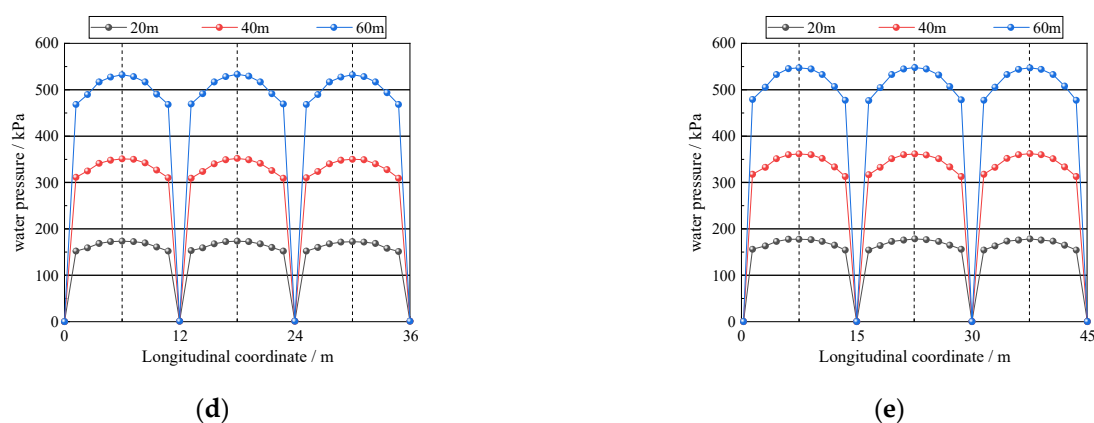
Figure 16. Distribution of water pressure at different water head heights and blind pipe spacing: (**a**) 3 m spacing; (**b**) 5 m spacing; (**c**) 8 m spacing; (**d**) 12 m spacing; (**e**) 15 m spacing.

Through the analysis of Figure 16, it can be seen that under different groundwater levels (20 m, 40 m, 60 m), as the spacing of the circumferential blind pipes increases, the pore water pressure at the arch crown within the interval gradually increases, and the peak water pressure appears near the middle of the interval. Taking the overlying water level of 60 m above the arch as an example, under the condition of blind pipe spacing of 3 m, the maximum pore water pressure at the arch top is 408.98 kPa, and taking the overlying water level of 60 m above the arch as an example, under the condition of blind pipe spacing of 3 m, the maximum pore water pressure at the arch top is 408.98 kPa. In addition, it can be seen that when the spacing between drainage blind pipes is small, the greater the decrease in water pressure at the unit axial distance from the blind pipe to the middle of the interval. Taking the overlying water level of 60 m above the arch as an example, under the condition of blind pipe spacing of 3 m, the average decrease in water pressure at the arch top per unit distance is 272.6 kPa, and when the spacing between drainage blind pipes increases to 15 m, the average decrease in water pressure at the arch crown per unit distance is 72.8 kPa. Meanwhile, through calculations, we can obtain the curve of the average water pressure of the secondary lining and inverted arch under different working conditions of the spacing between drainage blind tubes, as well as the variation curve of the average water pressure with the spacing between drainage blind tubes and the groundwater level, as shown in Figure 17.

(**a**)

(**b**)
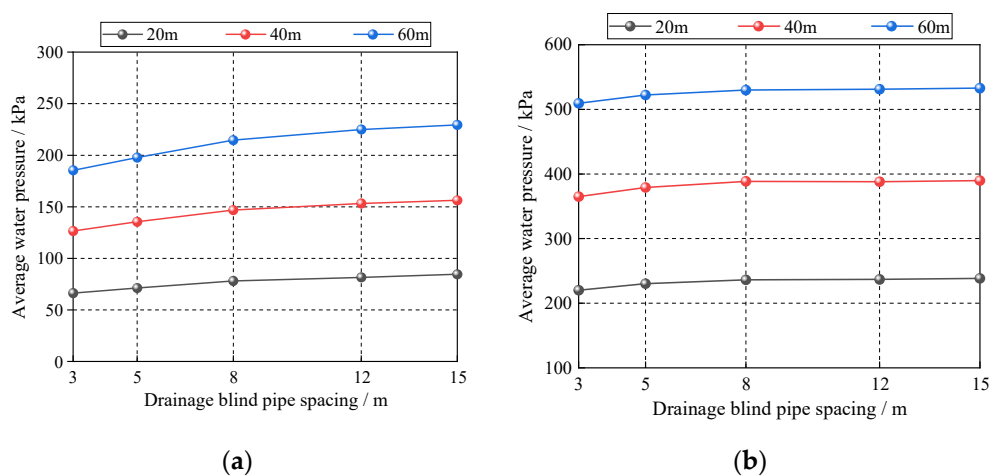
Figure 17. Curve of water pressure on lining surface as a function of drainage blind pipe spacing under different groundwater levels. (**a**) Average water pressure on the surface of the arch crown. (**b**) Average water pressure on the surface of the inverted arch.

As shown in Figure 17, through arranging circular and longitudinal drainage blind pipes, the water pressure acting on the surface of the secondary lining of the tunnel is less than the calculated water pressure to the groundwater level. This is because some of the groundwater on the surface of the secondary lining of the tunnel can be discharged through the drainage system, thereby reducing the average water pressure acting on the upper secondary lining and inverted arch. In addition, under the conditions of different water levels above the arch crown, the water pressure on the tunnel lining structure varies. The increase in groundwater level leads to an increase in the calculated water pressure from the surface of the secondary lining to the water level line, resulting in an increase in the pore water pressure of the surrounding rock around the tunnel, which causes the average water pressure acting on the surface of the lining structure will increase accordingly.

The analysis results indicate that if we want to achieve good pressure reduction through drainage, we should moderately reduce the spacing of drainage blind pipes. However, from the actual construction situation, designing overly dense spacing between circumferential blind pipes not only increases construction difficulty, but also increases engineering expenses, which does not meet the requirements of economy. Therefore, it is necessary to explore the optimal layout spacing of circular drainage blind pipes accordingly.

3.3.2. The Influence of the Spacing between Drainage Blind Pipes on the Water Pressure of the Lining

Due to the uneven distribution of water pressure behind the lining along the tunnel's circumferential and longitudinal directions, it is difficult to evaluate the pressure relief capacity of circular blind pipes with different spacing. So this article proposes the average water pressure $\overline{P}_p$, comparing the average water pressure in initial state $\overline{P}_{p0}$ with the average water pressure after blind pipe application $\overline{P}_{p1}$ to get the average pressure reduction coefficient φ.

The average pressure reduction coefficient φ can evaluate the weakening ability of blind pipes with different spacing on the water pressure behind the secondary lining. The smaller the coefficient φ, the greater its pressure relief capacity, and the smaller the residual pore water pressure behind the secondary lining.

The specific formula is as follows:

$$\overline{P}_p = \frac{\sum_{i}^{n} P_{zi} \times S_{zi}}{\sum_{i}^{n} S_{zi}} \tag{3}$$

$$\overline{\varphi} = \frac{\overline{P}_{p1}}{\overline{P}_{p0}} \tag{4}$$

In the formula, $\overline{P}_p$ is the average water pressure; $\overline{\varphi}$ is the average pressure reduction coefficient; $\overline{P}_{p0}$ is the average water pressure in initial state; $\overline{P}_{p1}$ is the average water pressure after blind pipe application; P_{zi} is the pore water pressure of unit i; S_{zi} is the water facing area of unit i; S_{zi} = unit volume/unit thickness.

Based on the average value of the water pressure acting on the surface of the secondary lining when the drainage blind pipe is arranged, which is obtained through numerical simulation, we can calculate the pore water pressure acting on the secondary lining surface when the blind drain is not arranged, calculate the corresponding reduction factor of the external water pressure of the lining under various working conditions $\overline{\varphi}$, and obtain

the water pressure reduction coefficient of the lining surface under different working conditions. From this, the variation curve of the water pressure reduction coefficient with the distance between the circumferential blind pipes under different groundwater level conditions can be plotted, as shown in Figure 18.

(**a**)   (**b**)
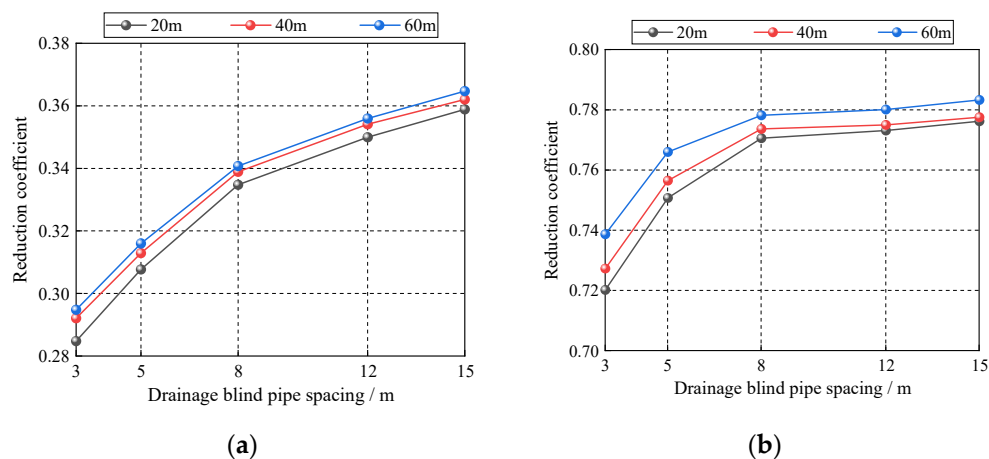
Figure 18. Change curve of water pressure reduction coefficient. (**a**) Reduction coefficient of water pressure on the surface of the arch crown. (**b**) Reduction coefficient of water pressure on the surface of inverted arch.

Through analyzing Figure 18, the following conclusions can be drawn.

Due to the arrangement of circular drainage blind pipes, the reduction coefficient of external water pressure in the upper part of the tunnel is significantly smaller. Under the condition of constant groundwater level, the reduction coefficient of external water pressure on the surface of the secondary lining under the spacing condition of each circumferential blind pipe is relatively small. Taking the condition of 60 m water level above the arch as an example, the maximum reduction coefficient of external water pressure on the surface of the secondary lining is 0.365, and the minimum is 0.294. The arrangement of circumferential blind pipes significantly reduces the average water pressure on the surface of the secondary lining. It can be seen that the surface water pressure can be effectively reduced using circumferential blind pipes, and the arrangement of blind pipes has good unloading capacity for external water pressure. Correspondingly, compared to the upper secondary lining, the drainage blind pipe has a weaker unloading capacity for the external surface water pressure of the inverted arch. Taking the 3 m blind pipe spacing as an example, during the process of increasing the water level above the arch from 20 m to 60 m, the reduction coefficients of external water pressure at the inverted arch are 0.723, 0.727, and 0.738, which are much greater than the reduction coefficients of water pressure at the arch crown.

Under the same circumferential blind pipe spacing conditions, the influence of groundwater level height on the water pressure reduction coefficient of the lining surface is relatively small. Taking the 3 m distance between circumferential drainage blind pipes as an example, during the process of increasing the water level above the arch from 20 m to 60 m, the water pressure reduction coefficients on the surface of the secondary lining are 0.285, 0.293, and 0.294, with an increase of 2.81% and 0.34%, respectively. The reduction coefficients of water pressure on the surface of the inverted arch are 0.723, 0.727, and 0.738, with an increase of 0.55% and 1.51%, respectively. From the results, it can be seen that the increase in water level above the arch crown has little effect on the reduction coefficient of water pressure on the lining surface, which can be almost ignored.

The change in the spacing arrangement of blind pipes for circumferential drainage will have an impact on the reduction coefficient of water pressure on the surface of the secondary lining. As the distance between blind pipes in circumferential drainage

increases, the unloading effect of blind pipes on water pressure becomes weaker, and the reduction coefficient of water pressure on the surface of the secondary lining becomes larger. Taking the condition of a water level 60 m above the arch as an example, when the spacing between the circumferential drainage blind pipes is 3 m, the reduction coefficient of water pressure on the surface of the secondary lining is 0.294, and as the distance between the circumferential drainage blind pipes increases, the reduction coefficient decreases in sequence. When the distance between the circumferential drainage blind pipes reaches 15 m, the reduction coefficient of water pressure on the surface of the secondary lining increases to 0.365, an increase of 24.1%. However, due to the fact that the circumferential blind pipe is not arranged at the inverted arch, the change in spacing has minimal impact on the reduction coefficient of external water pressure on the surface of the inverted arch, and the change in external water pressure on the surface of the inverted arch is not significant. Taking the overlying water level of the arch as an example, during the process of increasing the circumferential drainage blind pipe from 3 m to 15 m, the increase in the reduction coefficient of water pressure on the surface of the inverted arch is only 2.1%, far less than the 24.1% of the secondary lining arch crown.

3.3.3. Determination of the Optimal Spacing between Drainage Blind Pipes

According to the calculation and analysis, there must be reasonable spacing for the layout of blind pipes in the tunnel drainage system. Under this spacing condition, the drainage system not only has strong unloading capacity, but also does not cause construction difficulty and high cost due to dense spacing. Therefore, a point at the situation of the secondary lining of a tunnel usually produces cracks and seepage at the arch crown. We analyzed the water pressure reduction coefficient curve on the surface of the secondary lining to determine the optimal spacing of drainage blind pipes under different groundwater levels, as shown in Figure 19:
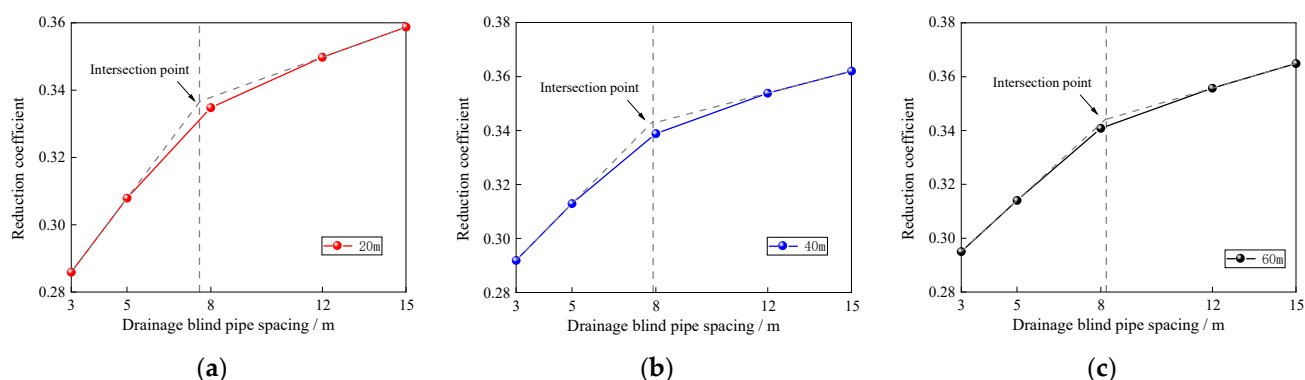
Figure 19. Change curve of water pressure reduction coefficient: (**a**) 20 m water level; (**b**) 40 m water level; (**c**) 60 m water level.

Find the intersection point of the straight line corresponding to the slope of the curve through the slope of the multi-point connecting line at both ends. The abscissa corresponding to this intersection point is the optimal blind pipe spacing value. And the analysis of the external water pressure reduction coefficient curve of the secondary lining shown in Figure 19 shows that during the process of densifying the layout of the circumferential drainage blind pipe, there is a turning point in the external water pressure curve of the secondary lining surface, which means that a slight densification of the circumferential blind pipe will cause a sharp decrease in the water pressure reduction coefficient. Therefore, at this point, it can be considered that the circumferential blind pipe spacing corresponding to this inflection point is the optimal layout spacing. At the same time, the inflection points under the water levels of 20 m, 40 m, and 60 m above the arch crown were obtained at 7.6 m, 7.9 m, and 8.2 m, respectively. However, due to the fact that in practical

engineering, the spacing between circumferential blind pipes is generally taken as an integer, the reasonable layout spacing of tunnel circumferential blind pipes during this operating period should be taken as 8 m.

Relevant literature was consulted when determining the spacing conditions. The research range of circumferential blind pipe spacing in these articles covers 3~10 m [23,24]. In addition, the circumferential blind pipe spacing of some water-rich tunnels is even 5 m [9], such as the Tiegalishan tunnel [8]. Therefore, the circumferential blind pipe spacing finally determined in this article is within a reasonable range.

The material of the circumferential blind pipe is PVC, which is relatively low-priced and easy to lay out. The density of circumferential blind pipes has little impact on the overall cost of the tunnel project. Moreover, the optimal circumferential blind pipe spacing determined in this article is only for the waterproof and drainage design of water-rich silty fine-sand-stratum sections, not for the entire tunnel. Adopting smaller blind tube spacing in special sections is more economical than repairing the structure after problems occur during the tunnel operation period. The economy of this plan is reasonable.

4. Study on the Safety of the Optimal Blind Pipe Spacing Secondary Lining during Operation Period

4.1. Bending Moment–Curvature Calculation Method

The bending moment–curvature relationship of support structures is commonly calculated using the fiber strip method. The fiber strip method is to divide the cross-section of reinforced concrete into several rectangular "strips" of the same area that are small enough based on the principle of differentiation, and at the same time, it is assumed that the strain within each long strip area is the same. Calculate the strain of each strip through the curvature of the structural cross-section, and then obtain its corresponding axial force through the constitutive relationship of the structure. Using the principle of superposition, the bending moment and axial force of each strip in the cross-section of the supporting structure component are concentrated to obtain the bending moment and axial force values acting on the overall component cross-section, and then the ultimate curvature of the component is obtained.

The internal force of the secondary lining structure of the tunnel during the operation period must be calculated in order to ensure the accuracy of the calculation results and simplify the calculation. Therefore, based on the commonly used assumption of a flat section in the calculation of reinforced concrete structures, the calculation is carried out. This method is based on the following: 1. The assumption of flat section; 2. neglecting the slip between steel bars and concrete; 3. neglecting the shear effect inside the component.

Based on the assumption of a flat section and the principles of material mechanics, the strain value at any point on the interface of reinforced concrete can be calculated using the following formula:

$$\varepsilon = \frac{y}{\rho} \tag{5}$$

$$\varepsilon_c = \frac{\xi_a h_0}{\rho} \tag{6}$$

In the formula, ε is the strain at any point of the component cross-section; y is the distance from any part of the component section to the neutral axis; $\frac{1}{\rho}$ is the curvature of the neutral layer of the component cross-section; ε_c is the strain of concrete at the edge of the compression zone of the component; ξ_a is the height of the relative boundary compression zone; h_0 is the section height.

According to Formulas (5) and (6), it can be inferred that the strain at any point in the cross-section of reinforced concrete components is directly proportional to its distance from the neutral axis.

For the calculation of reinforcement, Formula (7) is used to define the stress–strain constitutive curve of reinforcement. The stress–strain curve is shown in Figure 20.

$$\sigma_s = \begin{cases} E_s\varepsilon_s & \varepsilon_s \le \varepsilon_y \\ f_{y,r} & \varepsilon_y < \varepsilon_s \le \varepsilon_{uy} \\ f_{y,r} + k(\varepsilon_s - \varepsilon_{uy}) & \varepsilon_{uy} < \varepsilon_s \le \varepsilon_u \\ 0 & \varepsilon_s > \varepsilon_u \end{cases} \tag{7}$$
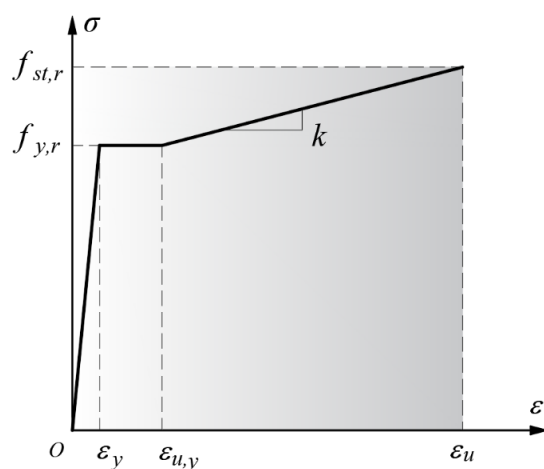

Figure 20. Stress–strain curve of steel bars.

In the formula, σ_s is the steel stress; E_s is the elastic modulus of steel bars; ε_s is the steel strain; $f_{y,r}$ is the calculation of the yield strength value of steel bars; ε_{uy} is the strain value at the starting point of the steel bar hardening section; ε_u is the peak strain of steel bars corresponding to the ultimate strength value of steel bars.

The uniaxial stress–strain constitutive relationship curve of concrete in the compression zone is determined according to Formulas (8)–(12). The stress–strain curve is shown in Figure 21.
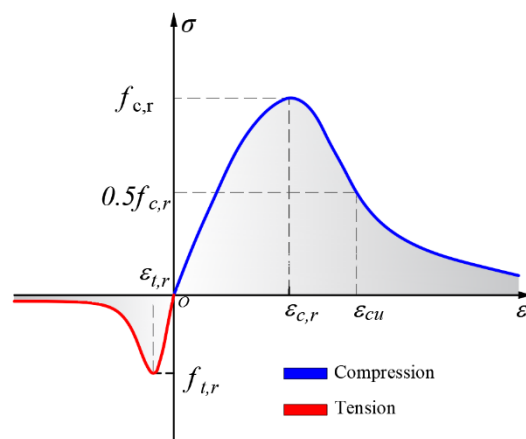
$$\sigma = (1 - d_c)E_c\varepsilon \tag{8}$$

$$d_c = \begin{cases} 1 - \dfrac{\rho_c n}{n - 1 + x^n} & x \le 1 \\ 1 - \dfrac{\rho_c}{\alpha_c(x-1)^2 + x} & x > 1 \end{cases} \tag{9}$$

$$\rho_c = \frac{f_{c,r}}{E_c\varepsilon_{c,r}} \tag{10}$$

$$n = \frac{E_c\varepsilon_{c,r}}{E_c\varepsilon_{c,r} - f_{c,r}} \tag{11}$$

$$x = \frac{\varepsilon}{\varepsilon_{c,r}} \tag{12}$$

Figure 21. Uniaxial stress–strain curve of concrete.

In the formula, d_c is the evolution parameters of concrete under uniaxial compression; α_c is the parameters of the descending section of the stress–strain curve of concrete under uniaxial compression; $f_{c,r}$ is the uniaxial compressive strength value of concrete; $\varepsilon_{c,r}$ is the peak compressive strain of concrete.

Based on the curvature, the stress at any point on the cross-section of the component can be calculated using the stress–strain constitutive relationship formula between steel bars and concrete, and the axial force and bending moment of the section can be calculated from this. Next, calculate the curvature of the reinforced concrete structural section based on the set constitutive relationship of reinforced concrete; the specific calculation flowchart is shown in Figure 22. First, the axial force and strain are randomly given based on the division of the strip. The axial force calculated based on the strain is compared with the given axial force to calculate the strain. Then, the curvature is calculated to determine whether it is damaged. If it is damaged, the strain and axial force are the limit values. Otherwise, the axial force is given again, and the above iterative calculation is performed.
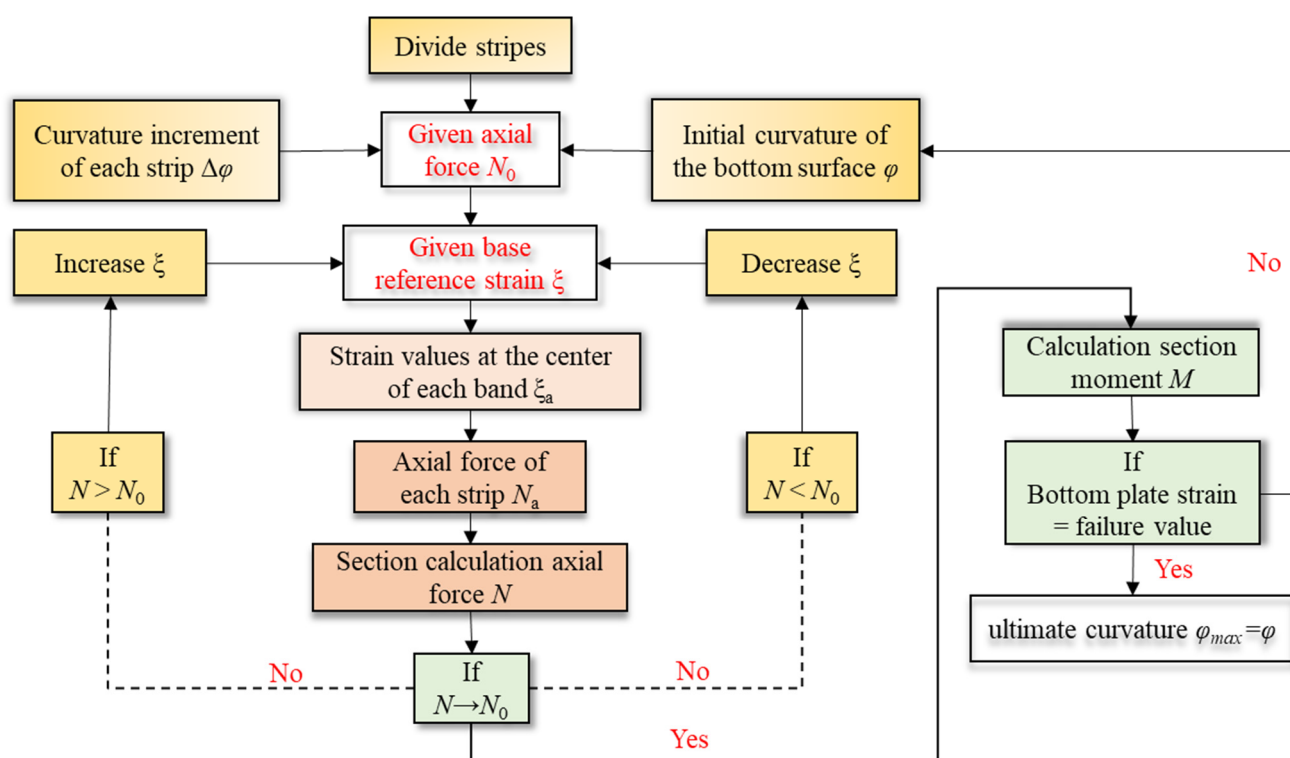
Figure 22. Calculation logic diagram of curvature–bending moment method.

The secondary lining of the tunnel is designed as water-pressure-resistant lining. The lining is made of a C35 reinforced concrete structure with a thickness of 0.65 m. The steel bars of the secondary lining components are HRB400 with a spacing of 20 cm, and the thickness of the protective layer of the steel bars is 5.5 cm. For the convenience of calculation, the calculation model takes a width of 1 m, and the adopted calculation model is shown in Figure 23. According to the calculation, the corresponding relationship between the bending moment and curvature transformation under different axial force conditions can be obtained. The bending moment–curvature relationship corresponding to different axial forces can be plotted as a curve as shown in Figure 24.
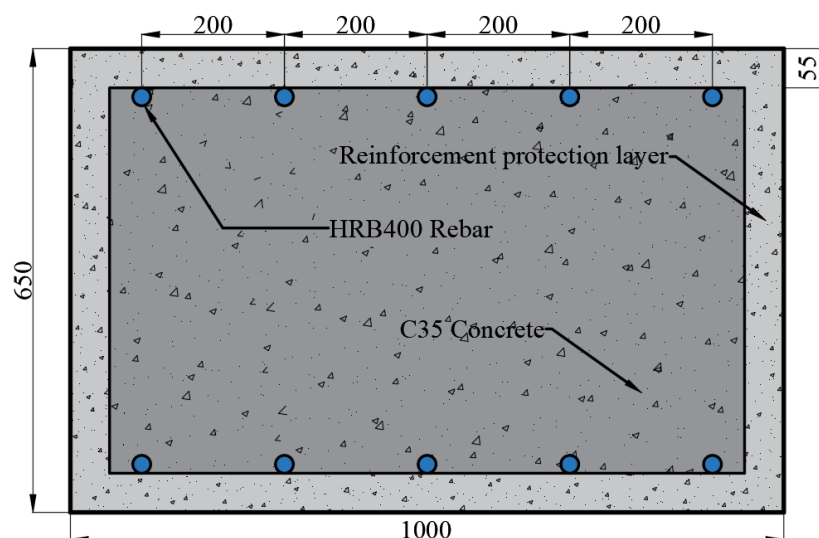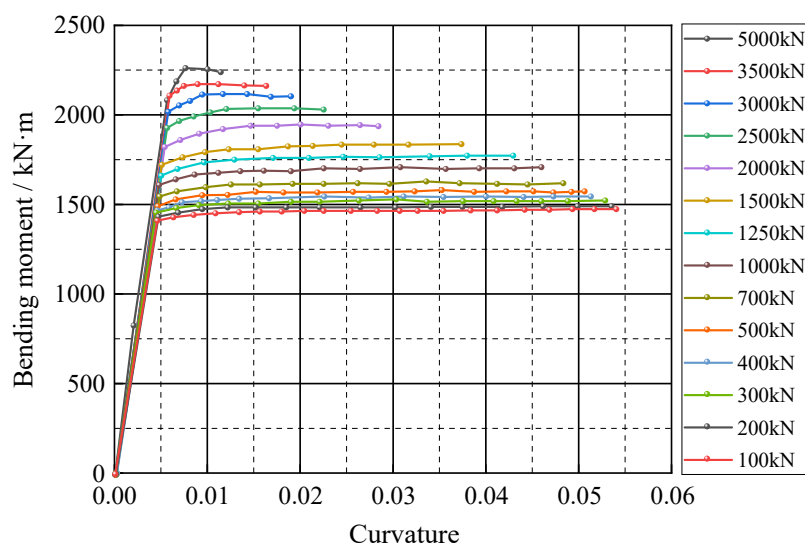

Figure 23. Schematic diagram of calculation model (unit: mm).

Figure 24. Bending moment–curvature relationship curve under different axial forces.

From Figure 24, it can be seen that there is a clear correlation between the bending moment and curvature corresponding to each axial force. Within a certain range, as the curvature increases, the bending moment shows a linear growth trend, indicating that the reinforced concrete components are in an elastic state at this stage. When the curvature increases to a certain value, the growth rate of the bending moment suddenly decreases, and then the bending moment hardly increases. The curve enters a horizontal state, indicating that the reinforced concrete component has already yielded and entered the plastic stage at this time. Therefore, this turning point can be considered as the yield point of the reinforced concrete components. After the component enters the plastic stage, it can be seen that the increase in curvature will not cause any further changes in the bending moment until the ultimate curvature. In addition, there is a negative correlation between the ultimate curvature and axial force, meaning that the ultimate curvature gradually decreases with the increase in axial force. A part of the calculation results of ultimate curvature and ultimate strain of lining structures under different axial forces can be summarized as shown in Table 3.

Table 3. Ultimate strain and curvature under different axial forces.

Axial Force (kN)	1500	2000	2500	3000	3500
Ultimate Curvature (10^{-2})	3.74	2.84	2.25	1.90	1.63
Ultimate strain of bottom plate (10^{-3})	4.37	4.38	4.38	4.89	4.06
Depth of compression zone (m)	0.1159	0.1541	0.1923	0.2578	0.2492

From Table 3, it can be seen that with the increase in axial force, the height of the compression zone of concrete components continuously increases; that is, the area of the compression zone of the component increases with the increase in axial force. At the same time, the calculated values of the ultimate strain of reinforced concrete components are greater than the specified ultimate compressive strain of concrete, indicating that the lining structure may first experience concrete crushing failure under bending moment action.

4.2. Numerical Simulation of Secondary Lining Safety Based on Bending Moment–Curvature

In engineering practice, due to the fact that technical personnel are usually unable to obtain accurate stress–strain parameters on site, they can only obtain limited relationship curves based on monitoring, such as the relationship between torsion angle and torque, the relationship between bending moment and rotation angle, and the relationship

between axial force and strain. The harsh monitoring conditions greatly hinder the monitoring of structural safety on the construction site. However, the ADINA finite element calculation software has its unique advantages in nonlinear calculations. It provides a simple method for directly defining the nonlinear properties of beam element materials: bending moment–curvature beams.

The characteristics of bending moment–curvature beams make them very suitable for simulating reinforced concrete structures in engineering, and they can better simulate the deformation and nonlinear characteristics of reinforced concrete lining under soil and water pressure. Thus, the calculation results of plastic curvature, axial force, and bending moment of the beam element can be obtained, which is convenient for studying the internal force of the reinforced concrete lining structure.

4.2.1. Establishment of Bending Moment–Curvature Beam Model

Generally speaking, the secondary lining is the last line of defense for tunnel waterproofing, and the safety of the secondary lining determines the long-term usability of the tunnel structure. Based on the characteristics of bending moment–curvature beams, the finite-element numerical simulation method is used to study the internal force and safety of the secondary lining structure of the tunnel during operation under the optimal drainage network layout. The specific numerical calculation parameters are shown in Table 4.

Table 4. Numerical calculation parameters table.

Category	Elastic Modulus E（GPa）	Poisson's Ratio μ	Cohesion C (MPa）	Friction φ (°)	Density ρ (kg/m³)	Unit Type
Rock	0.07	0.35	0.0037	31	1837	Plane-strain Unit
Curtain grouting area	0.8	0.31	0.12	35	2200	Plane-strain Unit
Initial support	28	0.2	-	-	2300	Plane-strain Unit
Secondary lining	31.5	0.2	-	-	2500	Elastic Unit
Secondary lining	-	-	-	-	-	Bending moment–Curvature Unit

In numerical calculations, the plane strain element is used to simulate the surrounding rock and initial support structure. The bending moment–curvature beam element and elastic beam element are respectively used to simulate the secondary lining for comparative analysis. The construction of tunnel excavation and support structures is simulated through defining the unit life and death at different times. The left and right boundaries of the calculation model are taken as 50 m from the side of the tunnel, and the distance from the bottom of the model to the bottom of the tunnel is 40 m. The overlying load is applied to the top of the model using a uniformly distributed load method. The specific calculation model is shown in Figure 25.


(**a**)   (**b**)
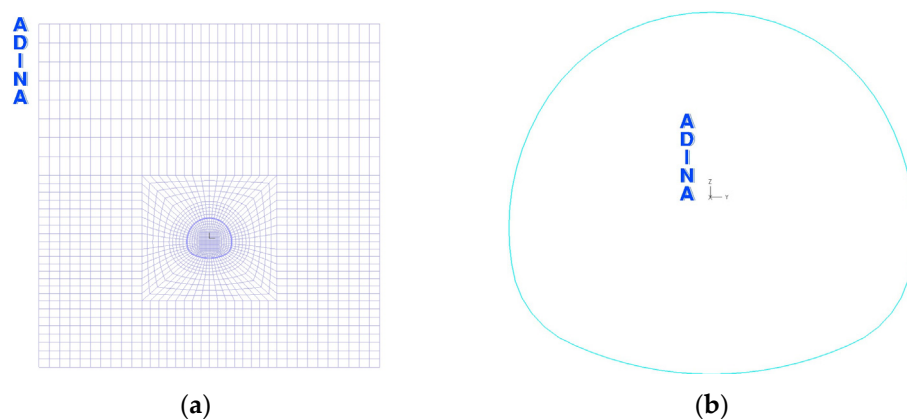
Figure 25. Schematic diagram of numerical calculation model. (**a**) Overall calculation model. (**b**) Beam unit second lining drawing.

The water pressure behind the secondary lining is directly applied by an external force vector. The specific values of the water pressure behind the secondary lining and the inverted arch are calculated using numerical methods and the average water pressure behind the lining during the operation period under the condition of reasonable drainage blind pipes. The water pressure on the top of the lining arch is 146.8 kPa, and the water pressure on the surface of the inverted arch is 388.6 kPa.

### 4.2.2. Numerical Calculation Results and Analysis

Through numerical calculation, the calculation results of the secondary lining structure defined by the bending moment–curvature beam and elastic beam under a simulated water-rich environment are shown in Figures 26 and 27.
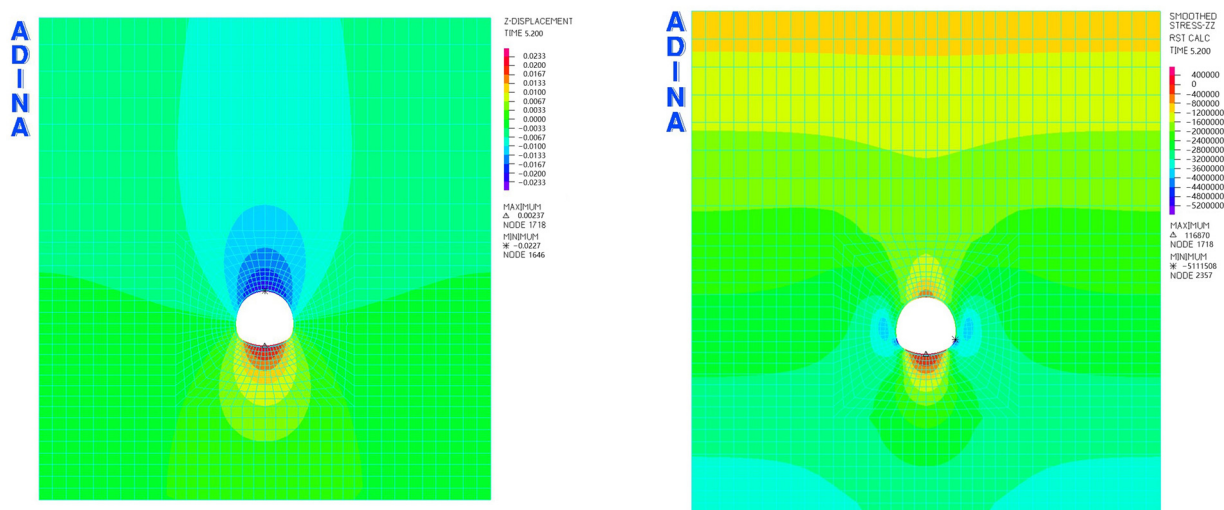
(**a**)

(**b**)

Figure 26. Cloud chart calculation results of elastic beam materials. (**a**) Elastic beam material displacement cloud map. (**b**) Stress nephogram of elastic beam material.
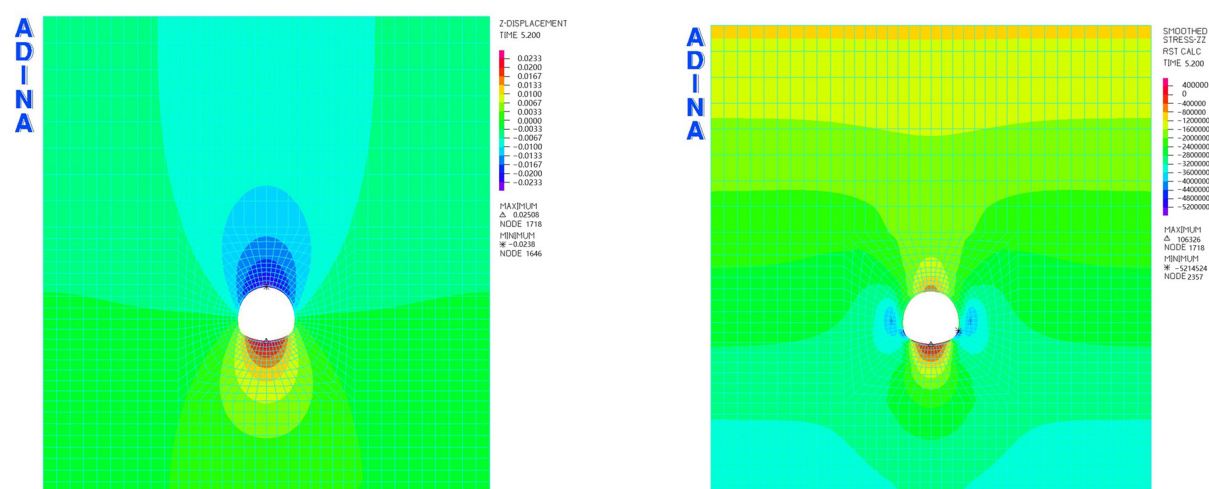

(**a**)

(**b**)

Figure 27. Calculation results of moment–curvature beam material cloud map. (**a**) Bending moment–curvature beam material displacement cloud chart. (**b**) Bending moment–curvature beam material stress cloud chart.

Through calculating the secondary lining element using the bending moment–curvature beam element and elastic beam element, respectively, it can be seen that the displacement and stress fields calculated using the bending moment–curvature beam element and elastic beam element are similar; that is because the material properties represented by the bending moment–curvature beam element and the elastic beam element are the same, so the overall results can be consistent. Extract the internal forces of the key parts of the secondary lining structure from the calculation results of elastic beam materials and bending moment–curvature beams, and draw internal force diagrams. According to the relevant provisions of Formulas (1) and (2) for the safety calculation of tunnel lining, the strength of the secondary lining structure is checked, and the safety coefficients of each key point are obtained as shown in Figure 28.
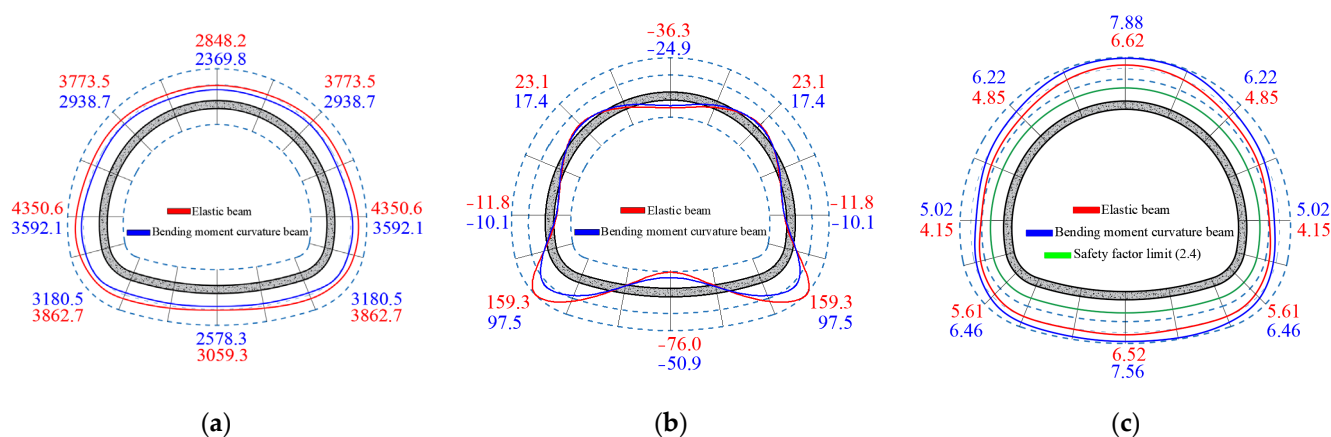
Figure 28. Internal force and safety factor of lining structure under different calculation methods. (**a**) Axial force (unit: kN); (**b**) bending moment (kN·m); (**c**) safety factor.

However, in terms of structural internal forces and internal force distribution, bending moment–curvature beams show differences compared to elastic beam elements. The axial force and bending moment of each key part of the elastic beam element structure are slightly larger than the calculation results of the bending moment–curvature beam element, while the internal force distribution of the bending moment–curvature beam element structure is more uniform than that of the elastic beam element. The calculation results show that the peak values of bending moment and axial force in the bending moment–curvature beam element and elastic beam element occur at the side wall and arch foot, respectively, and in the calculation results of the bending moment–curvature beam element, the maximum axial force is 3592.1 kN, which is 82.6% of the elastic beam condition, and the maximum bending moment is 97.5 kN·m, which is 61.2% of the elastic beam condition.

The safety factor calculation shows that the weak part of the secondary lining of the tunnel during the operation period is at the side wall, where the minimum safety factor of the bending moment–curvature beam element is 5.02, which is greater than that of the elastic beam element, 4.15, and all of them meet the regulations that the safety factor value is greater than 2.4, which means that the secondary lining is in a safe state. The calculation results indicate that through defining the relationship between the internal force and deformation of the structure to define the material, the bending moment–curvature beam element can better simulate the stress deformation characteristics of the lining structure.

The above results were compared and analyzed with the distribution rules of the internal force and safety factor of the lining structure before the optimized design of

waterproofing and drainage. It can be seen that the internal force distribution law of the lining structure under the optimal circumferential blind pipe spacing obtained through numerical simulation is similar to the on-site monitoring results. Under optimal blind pipe spacing, the drainage performance of the tunnel is better. The water pressure on the lining is reduced, which in turn makes the axial force of the lining structure smaller. Likewise, the overall bending moment of the lining structure is reduced. The minimum safety factor of the structure has changed from the original 3.04 and 3.17 to 5.02. Overall, the optimized structural stress state and safety are better.

The secondary lining safety evaluation method proposed in this article based on the bending moment–curvature method can directly calculate the internal force of the lining structure through the curvature of the lining structure, thereby evaluating its safety. In the practical application of this method, there is no need to embed sensors in the lining in advance to obtain the internal force of the structure. During tunnel construction and operation, the curvature changes of the lining structure can be monitored to evaluate structural safety.

5. Conclusions

This paper is based on the monitoring of water pressure, soil pressure, and structural internal forces in Taidacun Tunnel. The safety of the lining structure in the section of rich water, fine sand, and powder was evaluated using a numerical simulation method, the simulation of fluid structure coupling interactions under different water head heights, and circumferential blind pipe spacing conditions to determine the optimal circumferential blind pipe spacing. Furthermore, we analyzed the mechanical response of the lining structure under the optimized waterproof and drainage design system conditions. The main achievements of this study are as follows:

1. The structure of the Taidacun Tunnel bears significant soil and water pressure, especially in sections of water-rich and fine sand formations. The distribution pattern of soil pressure is characterized by a large arch crown and inverted arch compared to small side walls. The maximum earth pressure reaches 751.6 kPa. The water pressure gradually increases from the arch crown to the inverted arch, with the maximum water pressure reaching 359.2 kPa. The safety factor at the side wall of the tunnel lining in the water-rich and fine sand layer is relatively small, but the safety factors at all parts meet the specification requirements.

2. The minimum value of water pressure calculated through numerical simulation appears on both sides of the circumferential and longitudinal drainage blind pipes. At water levels of 20 m, 40 m, and 60 m, the maximum pore water pressures on the outer side of the secondary lining are 164.85 kPa, 334.75 kPa, and 506.05 kPa, respectively, and the calculated water pressure is smaller than the groundwater level line above the arch, which explicates that the installation of drainage blind pipes can reduce the maximum water pressure borne by the lining structure.

3. Through introducing the average pressure reduction coefficient index, the influence of the spacing of circumferential blind pipes on the water pressure borne by the lining was explored, and the optimal spacing of circumferential blind pipes in the water-rich area of the Taidacun Tunnel was determined to be 8 m. The pressure reduction coefficient at the arch crown is significantly greater than that at the inverted arch. The pressure reduction coefficient at the secondary lining arch crown is 0.29~0.37, and the pressure reduction coefficient at the inverted arch is 0.72~0.78.

4. A more practical safety evaluation method for secondary lining is proposed based on the bending moment–curvature beam model. Under the optimal spacing of drainage blind pipes, the bending moment–curvature beam can better characterize the mechanical characteristics of the secondary lining during the tunnel operation period, and the calculated internal force is smaller than that of the elastic beam calculation results. The safety factors of the secondary lining calculated using both methods are

greater than the specified minimum value of 2.4, and the minimum safety factor of the bending moment–curvature beam is 5.02, which is greater than 4.15 of the elastic beam element.

Author Contributions: Data curation, C.Z.; Funding acquisition, Z.Z. (Zhiqiang Zhang); Methodology, Z.Z. (Zelin Zhou), Z.Z. (Zhiqiang Zhang) and H.Z.; Project administration, Z.Z. (Zhiqiang Zhang); Software, Z.Z. (Zelin Zhou), X.Z., and C.Z.; Supervision, Z.Z. (Zhiqiang Zhang) and H.Z.; Validation, Z.Z. (Zelin Zhou) and X.Z.; Writing—original draft, Z.Z. (Zelin Zhou), X.Z., and C.Z.; Writing—review and editing, Z.Z. (Zelin Zhou), Z.Z. (Zhiqiang Zhang), and H.Z. All authors have read and agreed to the published version of the manuscript.

Data Availability Statement: The data used to support the findings of this study are available from the corresponding author upon request.

Conflicts of Interest: The authors declare no conflict of interest.

References

1. Zhang, Z.; Chen, B.; Li, H.; Zhang, H. The performance of mechanical characteristics and failure mode for tunnel concrete lining structure in water-rich layer. *Tunn. Undergr. Space Technol.* **2022**, *121*, 104335.
2. Yang, G.; Wang, G.; Lu, W.; Yan, P.; Chen, M. Damage assessment and mitigation measures of underwater tunnel subjected to blast loads. *Tunn. Undergr. Space Technol.* **2019**, *94*, 103131.
3. Bi, J.; Jiang, H.; Ding, W. Analytical solution for calculating the flow rate in a lined tunnel with drainage systems. *Tunn. Undergr. Space Technol.* **2023**, *138*, 105132.
4. Eichinger, S.; Boch, R.; Leis, A.; Koraimann, G.; Grengg, C.; Domberger, G.; Nachtnebel, M.; Schwab, C.; Dietzel, M. Scale deposits in tunnel drainage systems—A study on fabrics and formation mechanisms. *Sci. Total Environ.* **2020**, *718*, 137140.
5. Bao, T.; Zhang, S.; Liu, C.; Xu, Q. Experimental study on the effect of hydraulic deterioration of different drainage systems on lining water pressure. *Processes* **2022**, *10*, 1975.
6. Duan, S.; Jiang, X.; Jiang, Q.; Xiong, J.; Li, C. Theoretical solution and failure analysis of water pressure on lining of deep-buried non-circular hydraulic tunnel based on the equivalent hydraulic radius method. *Eng. Fail. Anal.* **2023**, *148*, 107163.
7. Fan, H.; Zhu, Z.; Song, Y.; Zhang, S.; Zhu, Y.; Gao, X.; Hu, Z.; Guo, J.; Han, Z. Water pressure evolution and structural failure characteristics of tunnel lining under hydrodynamic pressure. *Eng. Fail. Anal.* **2021**, *130*, 105747.
8. Zhang, C.; Liu, N.; Chen, K.; Ren, F. Study on drainage mode and anti-clogging performance of new waterproofing and drainage system in a tunnel. *Sci. Rep.* **2023**, *13*, 5354.
9. Zhao, D.; Fan, H.; Jia, L.; Song, Y. Research on waterproofing and drainage optimization scheme for karst tunnel lining in water-rich areas. *Environ. Earth Sci.* **2021**, *80*, 150.
10. Zhang, Z.; Huang, M.; Huang, J. Discussion on the design of water blocking and drainage limit of water-rich mountain tunnel in ecologically fragile area. *IOP Conf. Ser. Earth Environ. Sci.* **2020**, *510*, 052059.
11. Li, P.; Liu, H.; Zhao, Y.; Li, Z. A bottom-to-up drainage and water pressure reduction system for railway tunnels. *Tunn. Undergr. Space Technol.* **2018**, *81*, 296–305.
12. Wang, X.; Liu, L.; Fu, R.; Sun, X. Newly developed pressure adaptable concrete lining for high pressure hydraulic tunnels. *Tunn. Undergr. Space Technol.* **2020**, *105*, 103570.
13. He, B.; Xue, R.; Zhang, Z.; Feng, X.; Wu, C. A novel method of imposing external water pressure to explore the failure behavior of railway tunnel linings. *Tunn. Undergr. Space Technol.* **2023**, *133*, 104942.
14. Chen, Z.; Li, Z.; He, C.; Ma, C.; Li, X.; Chen, K.; Zhang, H.; Liu, M. Investigation on seepage field distribution and structural safety performance of small interval tunnel in water-rich region. *Tunn. Undergr. Space Technol.* **2023**, *138*, 105172.
15. Wu, Y.; Zhuang, G.; Liang, W.; Huang, L. Safety analysis of secondary lining of Yulinzi Tunnel based on field monitoring. *Appl. Sci.* **2023**, *13*, 8328.
16. Liu, S.; Shi, Y.; Sun, R.; Yang, J. Damage behavior and maintenance design of tunnel lining based on numerical evaluation. *Eng. Fail. Anal.* **2020**, *109*, 104209.
17. Song, W.; Lai, H.; Liu, Y.; Yang, W.; Zhu, Z. Field and laboratory study of cracking and safety of secondary lining for an existing highway tunnel in loess ground. *Tunn. Undergr. Space Technol.* **2019**, *88*, 35–46.
18. Guo, R.; Zhang, M.; Xie, H.; He, C.; Fang, Y.; Wang, S. Model test study of the mechanical characteristics of the lining structure for an urban deep drainage shield tunnel. *Tunn. Undergr. Space Technol.* **2019**, *91*, 103014.
19. Ding, Y.; Zhang, X.; Zhang, B. Preliminary study on double lining support design for water plugging of highway tunnel under high water pressure in mountain area based on limited drainage. *Appl. Sci.* **2022**, *12*, 7905.
20. Huang, M.; Yao, X.; Tan, Z.; Li, J. Research on Water Pressure Distribution Characteristics and Lining Safety Evaluation of Deep Shaft in Water-Rich, Large, Fractured Granite Stratum. *Appl. Sci.* **2022**, *12*, 7415.

21. China Academy of Architectural Engineering Co., Ltd. *Code for Design of Concrete Structures*; Construction Industry Press: Beijing, China, 2010. (In Chinese)
22. Chen, J.; Liu, X.; Zhang, W.; Zhang, J. Investigation and Statistical Analysis of Water Leakage in Highway Tunnels in Guizhou Province. *Mod. Tunn. Technol.* **2011**, *48*, 7–11. (In Chinese)
23. Fu, H.; An, P.; Li, K.; Cheng, G.; Li, J.; Yu, X. Grouting design of rich water tunnels and the calculation of distance between annular blind pipes. *Adv. Civ. Eng.* **2020**, *2020*, 8873971.
24. An, P.; Fu, H.; Chen, L.; Li, J. Analysis of water gushing after blockage of a drainage system in a deeply buried tunnel. *Hydrogeol. J.* **2022**, *30*, 2153–2162.